TECHNISCHE UNIVERSITÄT WIEN

Exploring possibilities for 2-butanol production in *A. woodii* by exchange of the ADH4 promoter

BACHELOR'S THESIS

submitted in partial fulfillment of the requirements for the degree of

Bachelor of Science

in

Technical Chemistry

by

Thomas Hackl
Registration Number 01526302

to the Research Group for Bioprocess Technology

at the TU Wien

Main advisor: Assistant Prof. Dipl.-Ing.(FH) Dr. Stefan Pflügl
Co-advisor: Projektasse(FWF) Dipl.-Inge Klara Wögerbauer, BSc

Vienna, October 21, 2025

Thomas Hackl | Stefan Pflügl

Declaration of Authorship

I hereby declare that I have written this Thesis independently, that I have completely specified the utilized sources and resources and that I have definitely marked all parts of the work - including tables, maps and figures - which belong to other works or to the internet, literally or extracted, by referencing the source as borrowed.

I further declare that I have used generative AI tools only as an aid, and that my own intellectual and creative efforts predominate in this work. In the appendix "Overview of Generative AI Tools Used" I have listed all generative AI tools that were used in the creation of this work, and indicated where in the work they were used. If whole passages of text were used without substantial changes, I have indicated the input (prompts) I formulated and the IT application used with its product name and version number/date.

Vienna, October 21, 2025

Thomas Hackl

Acknowledgements

I would like to sincerely thank my laboratory supervisor, Klara Wögerbauer, for her guidance and support throughout this thesis. In particular, I am grateful for her help with validating the presence of remaining wild-type strains by PCR and with integrating the 2-butanol peaks in Chromeleon. I also gratefully acknowledge Thomas Auzinger for providing the TU Wien Informatics Thesis Template, which I adapted for this thesis.

Abstract

The aim of this bachelor's project was to enhance the microbial production of 2-butanol from 2,3-butanediol by modifying the expression of alcohol dehydrogenase 4 (*adh4*) in *A. woodii*. To this end, the native promoter of *adh4* was replaced with the *pta* promoter from *Clostridium ljungdahlii* using the endogenous Type I-B CRISPR/Cas system of *A. woodii*. Homology-directed repair with specific spacer sequences enabled targeted integration. Plasmid constructs were assembled in *E. coli* and subsequently transformed into *A. woodii*. Correctly modified clones were confirmed via PCR and sequencing. Additionally, co-substrate experiments with 1,2-propanediol were performed to investigate whether its simultaneous addition could enhance 2-butanol formation by improving NAD^+ regeneration. The engineered strain was compared to the wild type under various substrate conditions, and product formation was analyzed by HPLC. While promoter replacement alone did not enhance 2-butanol production, the addition of 1,2-propanediol as a co-substrate resulted in a significant yet overall minor increase in 2-butanol yield, indicating that cofactor regeneration plays a role in the conversion of 2,3-butanediol to 2-butanol.

Contents

Abstract vii

Contents ix

1 Introduction 1
- 1.1 Acetobacterium woodii . . . 1
- 1.2 The Wood-Ljungdahl pathway . . . 2
- 1.3 2-Butanol metabolism . . . 2
- 1.4 CRISPR-based genome editing . . . 3
- 1.5 Golden Gate Cloning . . . 4
- 1.6 *A. woodii* Wild-type and Δ*aco1* Strains . . . 5
- 1.7 Aim of the work . . . 5

2 Materials and methods 7
- 2.1 Composition of stock solutions . . . 7
- 2.2 Preparation of Serum Bottles for Anaerobic Cultivation Experiments . . . 7
- 2.3 Preparation of Agar Plates . . . 8
- 2.4 Pre-cultivation of *A. woodii* Strains TU2.0 and Δaco1 . . . 8
- 2.5 Preparation of HPLC Standards . . . 9
- 2.6 Molecular Biology Methods . . . 9
- 2.7 Serum Bottle Experiments for 2-butanol Production Analysis . . . 11
- 2.8 Sampling and HPLC Sample Preparation . . . 12
- 2.9 Determination of 2-butanone and 1-propanol by Overlapping RI Peak Analysis . . . 12
- 2.10 Methodology for Carbon Balance Determination . . . 14

3 Results and Evaluation 17
- 3.1 Construction of the CRISPR array plasmid . . . 17
- 3.2 Transformation of the CRISPR array plasmid into *A. woodii* . . . 18
- 3.3 Serum Bottle Experiments for 2-butanol Production Analysis . . . 19

4 Discussion 29
- 4.1 Promoter Exchange of ADH4 in *A. woodii* . . . 29
- 4.2 Effect of 1,2-Propanediol on 2-Butanol Formation . . . 29
- 4.3 Carbon balance of mixed-substrate fermentations . . . 30
- 4.4 Hypothesis on the Preferential Use of the Wood-Ljungdahl Pathway under H_2 Conditions 30
- 4.5 Challenges in HPLC quantification of 2-butanol . . . 31
- 4.6 Outliers in Optical Density Measurements . . . 31

5 Outlook 33

List of Figures 35

List of Tables 37

Bibliography 39

Appendix A: HPLC Standards 43

Appendix B: Primer 45

Appendix C: Tools Used 47

CHAPTER 1

Introduction

The increasing demand for sustainable chemicals has highlighted the need for efficient microbial production of bio-based alcohols. 2-Butanol is an important platform chemical with applications as a fuel additive and in the chemical industry [Harvey and Meylemans, 2011, Song et al., 2019]. It can be produced chemically from petroleum, but bio-based production from renewable feedstocks is gaining attention due to environmental and economic considerations [Harvey and Meylemans, 2011, Russmayer et al., 2019]. Related compounds such as 2,3-butanediol and methyl ethyl ketone (MEK, 2-butanone) are also of industrial interest: 2,3-butanediol is used in chemical, cosmetic, agricultural, and pharmaceutical industries, and bio-based production processes have been developed to reduce reliance on expensive petrochemical routes [Kim et al., 2019], while MEK is widely employed as an industrial solvent and has potential as a fuel component [Torres-Vinces et al., 2020].

Among microbial hosts, *Acetobacterium woodii*, is capable of converting CO_2 and H_2 into a range of alcohols via the Wood–Ljungdahl pathway, making it a promising candidate for sustainable 2-butanol production [Balch et al., 1977, Ljungdhal, 1986, Wood, 1991]. Based on analogies with *Lentilactobacillus diolivorans*, which naturally converts meso-2,3-butanediol to 2-butanol [Russmayer et al., 2019], it is conceivable that carbon flux in *A. woodii* could similarly be redirected toward 2-butanol production. In particular, engineering strategies such as promoter modification of the alcohol dehydrogenase ADH4 may enhance the reduction of 2-butanone to 2-butanol. Together with advances in fermentation and metabolic engineering, *A. woodii* thus represents a promising platform for industrially relevant, bio-based alcohol production [Kim et al., 2019, Song et al., 2019].

1.1 Acetobacterium woodii

Acetobacterium woodii is a strictly anaerobic, gram-positive acetogen first isolated from marine sediments [Balch et al., 1977]. It utilizes the Wood-Ljungdahl pathway as its central metabolic route, enabling growth on H_2 and CO_2 as sole energy and carbon sources [Ljungdhal, 1986, Wood, 1991]. In addition to autotrophic growth, it can ferment a wide range of organic substrates such as fructose or lactate [Schoelmerich et al., 2018].

Widely present in anoxic ecological niches, including bottom sediments of seas and freshwater bodies, methanogenic communities, or hot springs, acetogens like *A. woodii* annually fix significant amounts of CO2 [Debabov, 2021]. The acetogenic metabolism is considered ancient, with the Wood-Ljungdahl pathway likely existing for up to 4 billion years [Martin, 2020].

Due to its robust anaerobic metabolism and well-characterized physiology, *A. woodii* has become a model organism for studying acetogenesis. It is considered non-pathogenic and safe to handle under laboratory conditions [Diekert, 1992]. Classical studies have demonstrated its metabolic flexibility, including the ability to produce ethanol and other alcohols under specific conditions, which makes it a promising candidate for biotechnological applications [Dangel et al., 1987, Drake, 1994].

Furthermore, *A. woodii* is genetically accessible, with established tools for targeted mutagenesis and promoter engineering, facilitating diverse metabolic engineering approaches. [Drake, 1994].

1.2 The Wood-Ljungdahl pathway

The Wood-Ljungdahl pathway (WLP), also known as the reductive acetyl-CoA pathway, is the central carbon fixation route in acetogenic bacteria such as *A. woodii*. It enables the conversion of CO_2 into acetyl-CoA, which serves as both a precursor for biomass formation and as a substrate for the synthesis of various metabolites [Ljungdhal, 1986, Wood, 1991, Fuchs, 1986], as illustrated in Figure 1.1

The pathway is divided into two branches: (i) the methyl branch, where CO_2 is sequentially reduced to formate and further converted to a methyl group bound to tetrahydrofolate, and (ii) the carbonyl branch, in which CO_2 is reduced to carbon monoxide by carbon monoxide dehydrogenase. Both branches converge at the acetyl-CoA synthase complex, which combines the methyl group, carbon monoxide, and coenzyme A to form acetyl-CoA [Ragsdale, 1991].

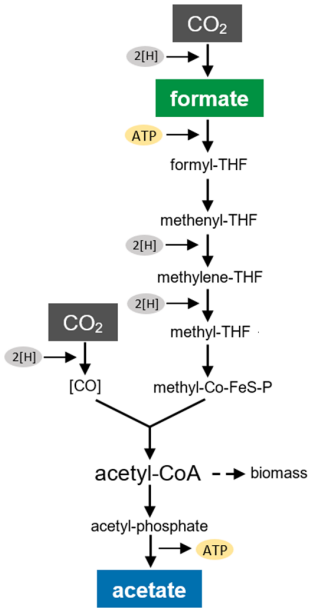


Figure 1.1: Schematic representation of the WLP in *A. woodii*, showing the methyl and carbonyl branches that come together in the formation of acetyl-CoA. Adapted from Klara Wögerbauer.

In *A. woodii*, the WLP not only supports autotrophic growth on CO_2 and H_2, but also provides a highly efficient route for energy conservation. The pathway couples the reduction of CO_2 to acetyl-CoA with the regeneration of reducing equivalents through electron bifurcation and establishes a sodium ion gradient that drives ATP synthesis via a Na^+-dependent ATP synthase. This makes the WLP a central metabolic hub for anaerobic growth and biomass formation in acetogens [Diekert, 1992, Drake, 1994].

1.3 2-Butanol metabolism

Alcohol dehydrogenases (ADHs) catalyze the reduction of ketones to alcohols and play a key role in 2-butanol biosynthesis. In *A. woodii*, ADH4 has been identified as a potential bottleneck for 2-butanol formation. Enhancing its expression through promoter engineering could increase product yield.

In wild-type *A. woodii*, 2,3-butanediol is partially oxidized to acetoin, which is subsequently metabolized by the Aco enzyme complex to acetaldehyde and acetyl-CoA (also $NAD^+ \rightarrow NADH$) [Fuchs, 1986, Diekert, 1992, Hess et al., 2015]. Part of the acetyl-CoA is converted to acetate with concomitant ATP formation.

2-Butanol formation is assumed to be linked to 2,3-butanediol metabolism by analogy to 1,2-propanediol degradation. In acetogenic bacteria, 1,2-propanediol is oxidized by the diol dehydratase complex PduCDE to propionaldehyde, which is subsequently reduced to 1-propanol by *adh4* using NADH [Oppermann et al., 1991, Schuchmann et al., 2015]. By analogy, 2,3-butanediol is converted to 2-butanone (MEK) by a similar enzymatic complex, followed by reduction to 2-butanol by *adh4*. Although the specific activity of *adh4* toward 2-butanone has not been experimentally determined, it has been suggested that this step could represent a rate-limiting conversion, potentially leading to intermediate accumulation and limited 2-butanol formation.

The enzyme PduQ belongs to the family of iron-dependent alcohol dehydrogenases (group III) and is evolutionarily specialized in the conversion of short-chain alcohols and aldehydes. Its characteristic function is the NAD^+-dependent oxidation of alcohols to aldehydes or, conversely, the NADH-dependent reduction of aldehydes to alcohols. Its physiological role was originally characterized in the context of 1,2-propanediol degradation in *Salmonella enterica*, where it is an integral component of a bacterial microcompartment (BMC) and essential for maintaining efficient metabolic flux through internal regeneration of NAD^+ from NADH [Cheng et al., 2012].

The overall pathway is summarized in Figure 1.2.

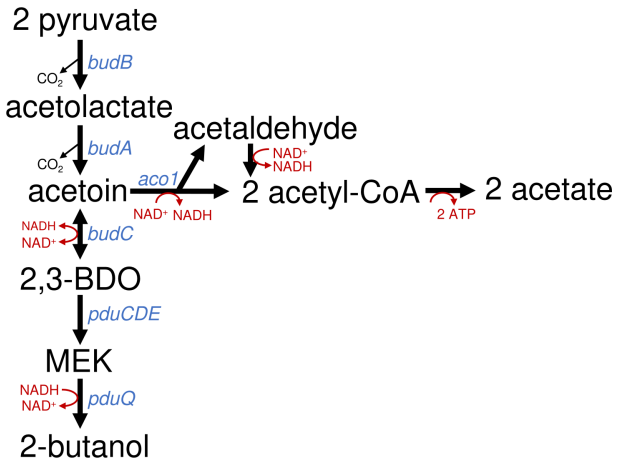


Figure 1.2: Schematic representation of 2,3-butanediol metabolism in *A. woodii*. 2,3-butanediol is oxidized by the PduCDE complex to 2-butanone (MEK), which can be reduced to 2-butanol by PduQ (ADH4). Simultaneously, 2,3-butanediol can be converted to acetoin by budC. Acetoin is degraded by Aco1 to one molecule of acetaldehyde and one molecule of acetyl-CoA; the acetaldehyde is subsequently oxidized to a second molecule of acetyl-CoA, with one acetyl-CoA molecule converted to acetate with concomitant ATP formation. Adapted from Klara Wögerbauer.

1.4 CRISPR-based genome editing

For genetic modifications in *A woodii*, the endogenous Type I-B CRISPR/Cas system offers an effective alternative to heterologous CRISPR-Cas9 systems, which are difficult to use in this organism because of nuclease toxicity and restriction barriers [Poulalier-Delavelle et al., 2023].

The approach uses an editing vector that carries a synthetic CRISPR array and a donor DNA template for homologous recombination. The synthetic array mimics the native arrays of *A. woodii*; it is controlled by the native leader sequence [Zhang et al., 2013, Moon et al., 2019, Poulalier-Delavelle et al., 2023] and contains a spacer (targeting the genomic locus of interest) flanked by direct repeats (DRs). Once expressed, the array is processed into crRNA, which guides the Cascade effector complex to the DNA target next to a protospacer adjacent motif (PAM). In Type I-B systems, PAMs often contain double cytosines [Boudry et al., 2015, Maikova et al., 2019]. In *A. woodii*, the functional PAM was identified as 5´-CCA-3´ [Poulalier-Delavelle et al., 2023]. After Cascade binding, the Cas3 nuclease is recruited and introduces a double-strand break near the target site [Mulepati and Bailey, 2013, Semenova et al., 2011, Wiedenheft et al., 2011].

The overall workflow of this mechanism is illustrated in Figure 1.3.

Using the endogenous CRISPR system for knock-in strategies such as promoter exchange demonstrates its potential for advanced metabolic engineering in the otherwise hard-to-edit acetogen *A. woodii* [Poulalier-Delavelle et al., 2023].

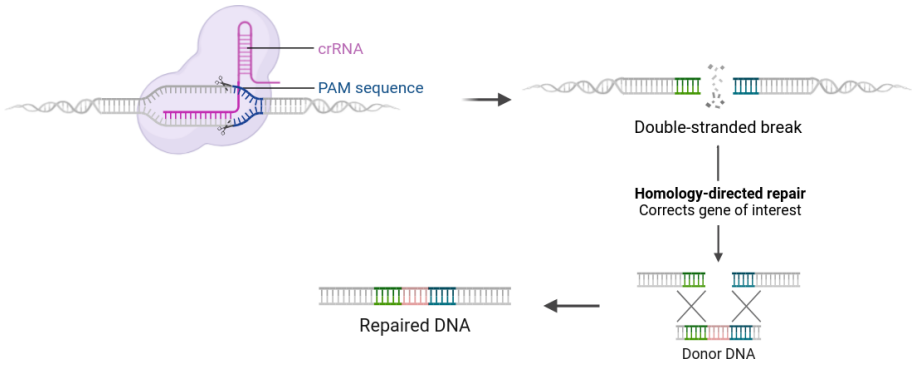


Figure 1.3: Schematic overview of the endogenous Type I-B CRISPR/Cas system mediated promoter replacement in *A. woodii*. A synthetic CRISPR array provides a crRNA that guides the Cascade complex to the target site next to a PAM sequence. Cas3 is then recruited and introduces a double-strand break in the genomic DNA. Homologous recombination with a donor DNA template containing the new promoter flanked by left and right homology arms (LHA and RHA) enables the integration of the modified sequence. (Adapted from a BioRender template by Esmée Dragt (biorender.com).)

This application of the endogenous CRISPR system for a knock-in strategy, such as promoter exchange, demonstrates its utility for advanced metabolic engineering in the genetically recalcitrant acetogen *A. woodii* [Poulalier-Delavelle et al., 2023].

1.5 Golden Gate Cloning

Golden Gate cloning is a versatile and efficient DNA assembly method that utilizes type IIS restriction enzymes, such as *BsaI* or *BpiI*, in combination with T4 DNA ligase [Engler et al., 2008, Weber et al., 2011]. Unlike conventional restriction enzymes, type IIS enzymes cut outside of their recognition site, generating user-defined overhangs that enable the seamless assembly of multiple DNA fragments in a predefined order, as illustrated in Figure 1.4.

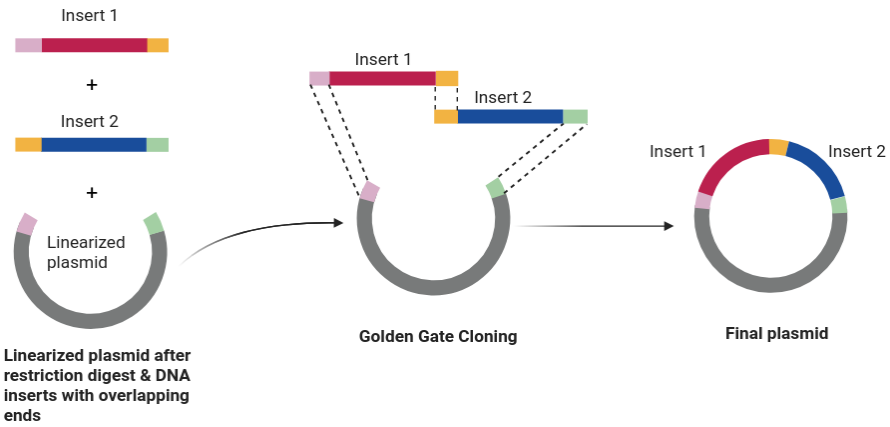


Figure 1.4: Schematic overview of the Golden Gate cloning process. (1) Linearized plasmid and DNA inserts with designed overhangs. (2) Complementary overhangs anneal. (3) T4 DNA ligase seals the nicks, yielding the final assembled plasmid. (Adapted from a BioRender template by Samara Ona (biorender.com).)

The method is performed in a single-pot reaction, where digestion and ligation occur simultaneously in a thermocycling program. This enables high efficiency and fidelity, as correctly ligated products no longer contain recognition sites for the restriction enzyme and are therefore protected from further cleavage [Engler et al., 2008].

Due to its modularity and efficiency, Golden Gate cloning has become widely used in synthetic biology and metabolic engineering for the rapid construction of plasmids, promoter libraries, and entire operons [Engler et al., 2014, Patron et al., 2015].

1.6 *A. woodii* Wild-type and Δ*aco1* Strains

The *A. woodii* TU2.0 strain serves as the wild-type control, expressing *adh4* under its native promoter.

The Δ*aco1* strain is a knockout mutant in which the *aco1* gene, encoding acetoin dehydrogenase, is disrupted (see Figure 1.2). This modification blocks the conversion of acetoin to 2-acetyl-CoA, thereby preventing the formation of acetate from 2,3-butanediol. Importantly, the Δ*aco1* strain retains the ability to convert 2,3-butanediol to 2-butanone, while the pathway leading to acetate formation is disrupted. This modification is therefore expected to redirect carbon flux toward 2-butanone and its subsequent reduction to 2-butanol.

1.7 Aim of the work

The aim of this work was to activate and enhance 2-butanol production in *A. woodii* and to evaluate the efficiency of different strains and promoter variants under various substrates and gas atmospheres. Specifically, the objectives were:

- Increase the expression of *adh4* by replacing its native promoter with (stronger) alternative promoters. This is intended to modulate the enzymatic reduction of 2-butanone to 2-butanol and direct the metabolic flux toward the desired alcohol.
- Investigate whether the simultaneous addition of 1,2-propanediol as a co-substrate to 2,3-butanediol stimulates 2-butanol production. The hypothesis is that the degradation of 1,2-propanediol produces both a carboxylic acid (propionic acid) and an alcohol (1-propanol), thereby regenerating NAD^+ from NADH. In contrast, the pathway from 2-butanone to 2-butanol does not generate a carboxylic acid, and thus no cofactor regeneration occurs. Providing both substrates simultaneously could improve the NADH/NAD^+ balance and facilitate the reduction of 2-butanone to 2-butanol.
- Evaluate the effect of molecular hydrogen on the cellular redox balance. It is assumed that the availability of H_2 provides additional reducing equivalents, enabling NADH/NAD^+ regeneration and thereby facilitating the conversion of 2-butanone to 2-butanol, increasing the overall production efficiency.

The study includes comparative analyses between the reference strains TU2.0 and Δ*aco1*, as well as their corresponding promoter-engineered variants TU2.0_Ppta and Δ*aco1*_Ppta. Where the substrates are identical, the reference and engineered strains are compared to determine the effect of promoter strength on 2-butanol production.

CHAPTER 2

Materials and methods

2.1 Composition of stock solutions

The stock solutions listed in Table 2.1 were used in the preparation of all defined and undefined media throughout this study.

Table 2.1: Composition of stock solutions used in all media.

Stock solution	Composition (per L)
10× phosphate A	KH_2PO_4 3.3 g, K_2HPO_4 4.5 g
10× phosphate B	KH_2PO_4 4 g, K_2HPO_4 4 g
10× salt A	NH_4Cl 10 g, NaCl 0.4 g, $MgSO_4 \cdot 7\,H_2O$ 2.2 g, $CaCl_2 \cdot 2\,H_2O$ 0.29 g, 100 µL Se-W stock
10× salt B	NH_4Cl 10 g, NaCl 1.2 g, $MgSO_4 \cdot 7\,H_2O$ 1.6 g, $CaCl_2 \cdot 2\,H_2O$ 0.02 g, 100 µL Se-W stock
Se-W stock (19 g/L)	$Na_2SeO_3 \cdot 5\,H_2O$ 0.97 g, $Na_2WO_4 \cdot 2\,H_2O$ 0.96 g (per 50 mL)
Fe stock (26.9 g/L)	$FeSO_4 \cdot 7\,H_2O$ 1.345 g (per 50 mL)
Resazurin stock (100 mL)	Resazurin sodium salt 0.002 g
TE 1000×	Nitrilotriacetic acid 15 g, $MnSO_4 \cdot H_2O$ 5 g, $CoCl_2 \cdot 6\,H_2O$ 1.52 g, $ZnSO_4 \cdot 7\,H_2O$ 1.8 g, $CuSO_4 \cdot 5\,H_2O$ 0.1 g, H_3BO_3 0.1 g, $Na_2MoO_4 \cdot 2\,H_2O$ 0.1 g, $NiSO_4 \cdot 6\,H_2O$ 0.33 g, $Na_2SeO_3 \cdot 5\,H_2O$ 0.003 g, $Na_2WO_4 \cdot 2\,H_2O$ 0.004 g

2.2 Preparation of Serum Bottles for Anaerobic Cultivation Experiments

Table 2.2: Ingredients for 1 L of the defined growth medium

Component	Amount
10x phosphate A	100 mL
10x salt A	100 mL
$NaHCO_3$	10 g
TE stock (1000x)	4 mL
Fe stock	0.074 mL
Resazurin stock	0.5 mL

The defined medium (Table 2.2) was prepared at the desired volume, with components proportionally scaled as needed. For the serum bottle experiments, 0.5 L of medium was prepared, supplemented

with $NaHCO_3$, Fe stock solution, and resazurin, and filled up to volume with deionized water. After filling, the solution appeared as a rich blue.

The flask was then degassed with an N_2/CO_2 gas mixture (flow rate: 0.5 L/min) in an 80:20 ratio. After a slight violet coloration, 0.25 g cysteine-HCl·H_2O was added, and degassing was continued until the medium took on a light pink color.

The serum bottles were then degassed for approximately 3 minutes. Using a dispensing device, 20 mL of the medium was added to each bottle, followed by an additional 3 minutes of degassing until the liquid exhibited only a faint pink hue. The bottles were then sealed with rubber stoppers, secured by crimped aluminum caps.

The solution completely lost its color after final autoclaving of the bottles.

2.3 Preparation of Agar Plates

Table 2.3: Composition of 1 L undefined medium for agar plates.

Component	**Amount**
10× Phosphate B	100 mL
10× Salt B	100 mL
Yeast Extract	1 g
$NaHCO_3$	3 g
TE 1000×	2 mL
Fe Stock	0.074 mL
Resazurin Stock	0.5 mL
Agar	15 g

The undefined medium (Table 2.3) was prepared at a volume of 0.5 L, with components proportionally scaled as needed. Agar plates were prepared by supplementing the medium with agar, TE buffer, Fe stock solution, and resazurin, and filling up to 0.5 L with deionized water. After preparation, the solution appeared as an intense blue.

The bottle was autoclaved and subsequently cooled down to a temperature suitable for the addition of the appropriate antibiotic for the bacterial strain (see Table 2.4). The medium was then dispensed into petri dishes within the laminar flow hood so that the bottom was just covered with liquid.

Table 2.4: Antibiotics used for the bacterial strains

Bacterial Strain	**Antibiotic (concentration)**
E. coli	Carbenicillin (100 µg/mL, from 1000× stock)
E. coli	Chloramphenicol (20 µg/mL, from 1000× stock)
A. woodii	Thiamphenicol (20 µg/mL, from 1000× stock)

2.4 Pre-cultivation of *A. woodii* Strains TU2.0 and Δaco1

Table 2.5: Composition of 1 L undefined medium

Component	Amount
10× phosphate A	100 mL
10× salt A	100 mL
Yeast extract	2 g
Sodium bicarbonate ($NaHCO_3$)	10 g

Continued on next page

Continued from previous page

Component	Amount
TE 1000×	2 mL
Fe stock solution	0.037 mL
Resazurin stock solution	0.5 mL

The undefined growth medium (Table 2.5) was prepared at a volume of 0.5 L, with components proportionally scaled as needed. The medium was supplemented with Fe stock solution and resazurin, and filled up to 0.5 L with deionized water. Upon preparation, the solution assumed a deep blue color.

Degassing of the medium and preparation of the serum bottles were performed analogously as described in Section 2.2.

Finally, 1 mL of each prepared cell culture was injected into separate serum bottles using a sterile syringe: one bottle contained *A. woodii* strain TU2.0, and the other contained strain Δaco1. The cultures were then incubated in a shaking incubator at 30 °C and 100 rpm.

2.5 Preparation of HPLC Standards

HPLC (High-performance liquid chromatography) standards were prepared gravimetrically, without using stock solutions. For each target concentration, the required amount of pure compound was calculated using the molar mass, the desired concentration, and the target volume, according to equation 2.1. When necessary, the purity of the compound was also taken into account. The calculated amount of each standard was weighed using an analytical balance, dissolved in deionized water, and brought to a final volume using a volumetric flask (typically 10–25 mL, chosen to facilitate convenient handling and accurate weighing).

$$m = c \cdot V \cdot \frac{M}{P} \tag{2.1}$$

where:
m = required mass of the substance [g]
c = target concentration of the solution [mol/L or g/L]
V = final volume of the solution [L]
M = molar mass of the substance [g/mol]
P = purity of the substance (e.g., 0.98 for 98% purity)

All calibration standards prepared for this study are listed in the Appendix (Appendix A).

2.6 Molecular Biology Methods

2.6.1 Construction of the CRISPR array plasmid

In this study, a donor plasmid was constructed via Golden Gate assembly to serve as a template for the endogenous Type I-B CRISPR/Cas system in A. woodii. The plasmid contained left and right homology arms (LHA and RHA) flanking the new promoter sequence, allowing precise replacement of the native *adh4* promoter with (stronger) variants. Additionally, it carried a synthetic CRISPR array that produces crRNAs to guide the native Cascade complex and Cas3 nuclease to the correct genomic target site for DNA cleavage and homologous recombination.

In the first step of constructing the CRISPR array, the primer pairs KWO_124/KWO_125 (for spacer gRNA 1) and KWO_126/KWO_127 (for spacer gRNA 2) (Appendix B) were annealed by cooling from 95 °C to 25 °C over 10 minutes. For each spacer, 1 µl of both primers was mixed with 48 µl

of water to obtain a final concentration of 200 nM. This process anneals the primers to form the double-stranded spacer, which was then used in the assembly of the CRISPR array.

In the meantime, the homologous regions (LHA and RHA; primers KWO_128 / KWO_129 and KWO_134 / KWO_135) (Appendix B), the promoter of the *AWO_RS05465* gene (RS05; primers KWO_132 / KWO_133) (Appendix B), and the pta promoter from the *Clostridium ljungdahlii* genome (primers KWO_131 / KWO_130) (Appendix B) were amplified by PCR using the B7 High Fidelity DNA Polymerase (Biozym Scientific GmbH, Hessisch Oldendorf, Germany) according to the manufacturer's protocol.

To verify the PCR products, agarose gel electrophoresis was performed. For gel preparation, 0.4 g of agarose were dissolved in 50 mL of 1× TAE (TRIS-Acetat-EDTA) buffer by heating the mixture in a microwave until the agarose was fully melted (approximately 1 minute), and subsequently stained with 3 µL of SYBR™ Safe DNA Gel Stain (Thermo Fisher Scientific, Waltham, MA, USA). After casting the gel, the PCR products were loaded alongside a 1 kb Plus DNA ladder (Thermo Scientific™ GeneRuler) and run at 100 V for approximately 45 minutes.

Next, the two spacers were cloned into separate plasmids (spf-2042) using Golden Gate assembly and subsequently transformed into *E. coli* by heat shock. Selection was performed on LB agar plates supplemented with carbenicillin, as the plasmid backbone carries an carbenicillin resistance gene.

The overnight-grown cells were screened for the presence of the two spacers by colony PCR using the YourTaq™ Direct-Load PCR Master Mix (biotechrabbit GmbH, Berlin, Germany), followed by gel electrophoresis. Spacer 1 was amplified with primers KWO_113 and KWO_125, and spacer 2 with primers KWO_113 and KWO_127. Plasmid DNA from positive clones was isolated using the HiYield Plasmid Mini Kit (SLG GmbH, Germany) according to the manufacturer's protocol, and the correct assembly and completeness of the plasmid were validated through Sanger sequencing. Positive clones were then used to inoculate 3 mL overnight cultures in culture tubes containing LB medium supplemented with carbenicillin.

In the second step of constructing the CRISPR array, the DNA fragments for LHA, RHA, the promoters, and the spacer region (cloned into the spf-2042 plasmid) were assembled into the *E. coli* spf-3051 plasmid using Golden Gate assembly. Two separate plasmids were constructed: one containing the pta promoter and the other containing the promoter of the *AWO_RS05465* gene. These plasmids were subsequently transformed into *E. coli* via heat shock. Selection was performed on LB agar plates supplemented with chloramphenicol, as the plasmid backbone (spf-3051) confers resistance to chloramphenicol. Overnight-grown clones were screened by colony PCR using primers REY_007 and REY_008 (Appendix B) with biotechrabbit YourTaq™ Direct-Load PCR Master Mix, followed by gel electrophoresis to verify the presence of the homologous regions and promoters. Additionally, the constructs were verified by Sanger sequencing.

After confirming the completeness of the plasmid, an overnight culture was started in a 250 mL Erlenmeyer flask containing 50 mL of LB medium supplemented with chloramphenicol, and the plasmid DNA was isolated using the NucleoBond® Xtra Midi kit (Macherey-Nagel GmbH & Co. KG, Düren, Germany), following the manufacturer's instructions.

2.6.2 Transformation of the CRISPR array plasmid into *A. woodii*

Transformation of *A. woodii* was performed via electroporation under strictly anaerobic conditions, using an internal protocol (K. Wögerbauer, *Acetobacterium woodii* transformation, 2024) adapted from the method of Poulalier-Delavelle et al. [Poulalier-Delavelle et al., 2023].

Cells were grown overnight to an OD_{600} of approximately 0.35 in fructose- and vitamin-supplemented medium. After harvesting by centrifugation, the cells were washed with ice-cold SMP buffer and concentrated to a final volume of 200 µL per transformation.

Electroporation was carried out using 200 µL of competent cells and approximately 10 µL of plasmid DNA in a 1 mm cuvette with the following parameters: 1.0 kV, 200 Ω, 50 µF (time constant ∼6–9 ms).

Immediately after the electric pulse, 1 mL of recovery medium was added, and the mixture was transferred into a Hungate tube containing 9 mL of the pre-reduced undefined growth medium (see Table 2.5). Tubes were flushed with N_2/CO_2 and incubated anaerobically at 30 °C for 6 h.

After regeneration, cells were plated on selective agar medium supplemented with cysteine and thiamphenicol, with TU2.0 and Δ*aco1* transformations on separate plates. All plates were incubated together in an anaerobic box (GasPak system) until colonies appeared, requiring up to 12 days. From each plate, a single colony was picked and consecutively numbered (colonies 1–6 for TU2.0, colonies 7–12 for Δ*aco1*) and inoculated into antibiotic-free liquid medium in well plates. After 2 days of cultivation, lysates were prepared by heat treatment at 100°C, and colony PCR was performed using B7 High Fidelity DNA Polymerase with primers KWO_139 and KWO_137 (Appendix B) to screen for colonies showing the expected 1600 bp band.

2.6.3 Strains and plasmids used in this study

Table 2.6 lists all A. woodii strains used in this study

Table 2.6: *A. woodii* strains used in this study.

Short name	Full designation	Description
TU2.0	TU2.0	Wild-type strain, expresses *adh4* under native promoter
Δ*aco1*	Δ*aco1*	Knockout of *aco1*, acetoin dehydrogenase disrupted
TU2.0_Ppta	TU2.0 P_{adh4}::P_{pta}	Promoter replacement, *adh4* under *pta* promoter
Δ*aco1*_Ppta	Δ*aco1* P_{adh4}::P_{pta}	Knockout strain with promoter replacement

2.7 Serum Bottle Experiments for 2-butanol Production Analysis

20 mL of defined medium (CDM) were dispensed into serum bottles and, under anaerobic conditions, supplemented by syringe injection with 0.4 mL of a vitamin solution, 2,3-butanediol as the main carbon source, and either propanediol, ethylene glycol, or methanol as cosubstrates. 1 mL Precultures of the strains TU2.0 or Δ*aco1* were inoculated into the bottles (see Table 2.7).

Table 2.7: Codes and details for serum bottles with strains expressing native promoter (strain, carbon source and gas phase).

Code	Strain	C-source	Gas phase
A – C	TU2.0	2,3-butanediol (20 mM)	N_2/CO_2
D – F	TU2.0	2,3-butanediol (20 mM) + methanol (50 mM)	N_2/CO_2
G – I	Δ*aco1*	2,3-butanediol (20 mM)	N_2/CO_2
J – L	Δ*aco1*	2,3-butanediol (20 mM) + methanol (50 mM)	N_2/CO_2
M – N	TU2.0	2,3-butanediol (20 mM) + 1,2-propanediol (15 mM)	N_2/CO_2
O – P	TU2.0	2,3-butanediol (20 mM) + ethylene glycol (20 mM)	N_2/CO_2
Q – R	Δ*aco1*	2,3-butanediol (20 mM) + 1,2-propanediol (15 mM)	N_2/CO_2
S – T	Δ*aco1*	2,3-butanediol (20 mM) + ethylene glycol (20 mM)	N_2/CO_2

For the transformed *A. woodii* strains, the preparation of serum bottles was carried out analogously; however, the experimental setup was modified. While triplicate samples remained unchanged, the duplicate samples were incubated under a hydrogen atmosphere and with different carbon sources, as detailed in Table 2.8.

Table 2.8: Codes and details for serum bottles with transformed *A. woodii* strains expressing the *pta* promoter (strain, carbon source and gas phase).

Code	Strain	C-source	Gas phase
pA – pC	TU2.0_Ppta	2,3-butanediol (20 mM)	N_2/CO_2
pD – pF	TU2.0_Ppta	2,3-butanediol (20 mM) + methanol (50 mM)	N_2/CO_2
pG – pI	Δ*aco1*_Ppta	2,3-butanediol (20 mM)	N_2/CO_2
pJ – pL	Δ*aco1*_Ppta	2,3-butanediol (20 mM) + methanol (50 mM)	N_2/CO_2
H1 – H2	TU2.0_Ppta	2,3-butanediol (20 mM)	H_2
H3 – H4	TU2.0_Ppta	2,3-butanediol (20 mM) + methanol (50 mM)	H_2
H5 – H6	TU2.0_Ppta	2-butanone (20 mM) + 1,2-propanediol (15 mM)	H_2

2.8 Sampling and HPLC Sample Preparation

To monitor cell growth and anaerobic conditions, optical density was measured at 600 nm (OD_{600}) and 660 nm (OD_{660}) using a ONDA V-10 Plus UV/VIS spectrophotometer (ONDA, Milan, Italy), respectively. For this purpose, 1 mL of culture was withdrawn directly from the serum bottle using a sterile syringe. After OD measurement, the same sample was used for HPLC preparation.

For HPLC analysis, the 1 mL sample was centrifuged at 21,000 × g for 10 minutes. The supernatant was transferred to a fresh tube, and the cell pellet was discarded. Subsequently, 540 µL of the supernatant were mixed with 60 µL of 40 mM sulfuric acid, vortexed thoroughly, and centrifuged again at 21,000 × g for 10 minutes. A volume of 540 µL of the clarified sample was transferred into an HPLC vial for analysis.

HPLC analysis was performed using a Vanquish Core HPLC system equipped with a Vanquish Variable Wavelength Detector F and a Refractomax520 detector (Thermo Fisher Scientific, Wilmington, United States). Separation was carried out on an Aminex HPX-87H column (Bio-Rad, Hercules, United States). The mobile phase consisted of 4 mM sulfuric acid (H_2SO_4) at a flow rate of 0.6 mL/min and a column temperature of 60 °C. A sample volume of 10 µL was injected, and each run lasted 45 minutes. Detection was performed primarily using a refractive index (RI) detector, with additional UV detection at 280 nm. Data analysis was conducted using Chromeleon CDS software (Thermo Fisher Scientific, Wilmington, United States).

Further data analysis and visualization were performed using Python (version 3.12.3).

2.9 Determination of 2-butanone and 1-propanol by Overlapping RI Peak Analysis

The peak of 1-propanol overlaps with the peak of 2-butanone in the refractive index (RI) spectrum due to identical retention times, which complicates the quantification of both 2-butanone and 1-propanol. Therefore, butanone was quantified based on its UV280 absorption spectrum.

Figure 2.1 shows the calibration curve for 2-butanone, created from the RI data by performing linear regression of the measured concentrations and their corresponding peak areas.

Equation (2.2) was used to convert the butanone concentration determined from the UV280 measurement into an equivalent RI peak area.

$$A_{\mathrm{MEK}} = 0.0975 \cdot C_{\mathrm{MEK}}^{\mathrm{UV}} - 0.0371 \tag{2.2}$$

where:
A_{MEK} = Peak area of 2-butanone in RI spectrum
$C_{\mathrm{MEK}}^{\mathrm{UV}}$ = Concentration of 2-butanone measured by UV280

Equation (2.3) was used to calculate the concentration of 1-propanol by subtracting the calculated butanone peak area from the total peak area (2-butanone + 1-propanol) to isolate the peak area corresponding to 1-propanol.

$$A_{\mathrm{C3}} = A_{\mathrm{total}} - A_{\mathrm{MEK}} \tag{2.3}$$

where:
A_{C3} = Peak area of 1-propanol in RI spectrum
A_{total} = Total peak area of 1-propanol and 2-butanone in RI spectrum
A_{MEK} = Peak area of 2-butanone in RI spectrum

Finally, the remaining RI peak area was converted back into a 1-propanol concentration using the calibration curve obtained from a 1-propanol standard (Equation (2.4), Figure 2.2).

$$C_{\mathrm{C3}} = \frac{A_{\mathrm{C3}} + 0.0178}{0.0812} \tag{2.4}$$

where:
C_{C3} = Concentration of 1-propanol
A_{C3} = Peak area of 1-propanol in RI spectrum

This approach allows the separation of overlapping peaks in the RI spectrum and enables accurate quantification of both compounds.

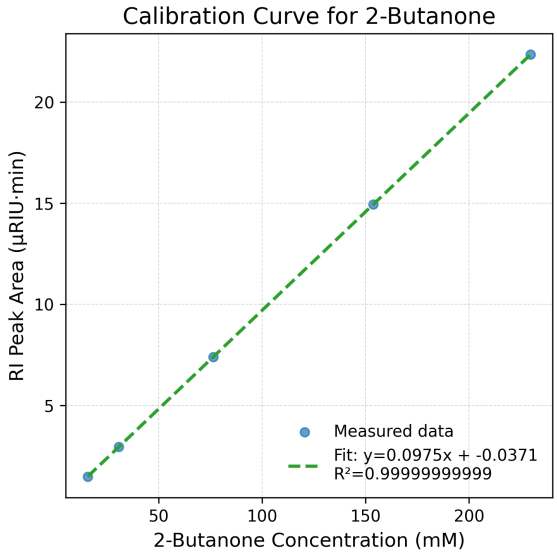


Figure 2.1: Linear regression of refractive index (RI) peak areas against known 2-butanone concentrations. The resulting calibration equation allows conversion of concentrations determined from UV280 spectra into expected RI peak areas.

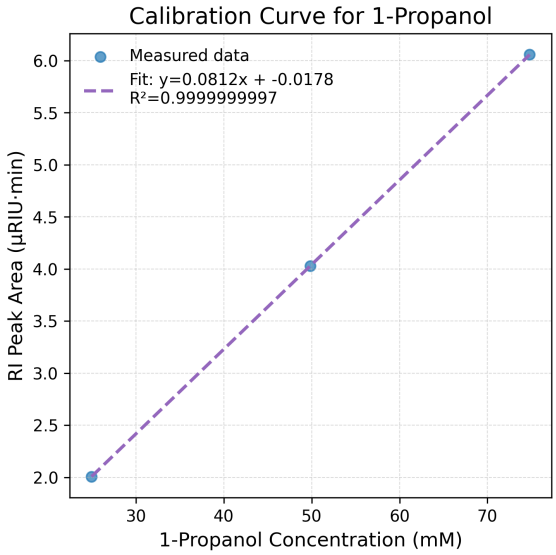


Figure 2.2: Linear regression of the calibration curve for 1-propanol, relating RI peak areas to known concentrations. The resulting regression equation enables conversion of calculated peak areas into concentrations.

2.10 Methodology for Carbon Balance Determination

To evaluate the distribution of carbon during fermentation, a carbon mass balance was performed. The carbon content of each detected soluble product was calculated by multiplying its molar concentration with the respective number of carbon atoms per molecule (see Table 2.9). The total amount of carbon recovered in the fermentation products and biomass was then compared to the initial amount of carbon introduced with the substrate. For comparative purposes, the total input carbon was normalized to 1, allowing for a relative assessment of carbon recovery across different experimental conditions.

It should be noted that carbon present in the form of CO_2 or carbonate may also contribute to the overall carbon balance but was not considered in this calculation.

Table 2.9: Overview of relevant compounds used for carbon balancing. The number of carbon atoms per molecule was used to calculate mmol of carbon from measured concentrations.

Compound	Molecular Formula	C Atoms / Molecule
2,3-Butanediol	$C_4H_{10}O_2$	4
Acetate	$C_2H_4O_2$	2
2-Butanone	C_4H_8O	4
Propionate	$C_3H_6O_2$	3
1-Propanol	C_3H_8O	3
Ethylene glycol	$C_2H_6O_2$	2
Methanol	CH_4O	1
Ethanol	C_2H_6O	2
1,2-Propanediol	$C_3H_8O_2$	3
Biomass	$C_1H_{1.934}N_{0.228}S_{0.0058}O_{0.593}P_{0.028}$	–
Propionaldehyde	C_3H_6O	3

To estimate the carbon content of the biomass, the optical density at 600 nm (OD600) measured in Section 2.8 was used. For *A. woodii*, an empirical conversion factor of 0.38 g/L (cell dry weight, CDW) per unit of OD600 was applied [Neuendorf et al., 2021], as shown in Equation 2.5.

$$CDW = OD600 \cdot 0.38 \ \frac{g}{L} \tag{2.5}$$

The carbon mass in the biomass was subsequently calculated assuming a carbon content of 45% (w/w) of the dry weight [Godley et al., 1990], using Equation 2.6. In this calculation, a molecular weight of 12 g/mol was used for carbon, and a conversion factor of 1000 was applied to convert from g/L to mmol/L. This approximation allows a rough estimation of the biogenic carbon distribution in the system.

$$\mathrm{C_{biomass}} = \mathrm{CDW} \cdot 0.45 \cdot \frac{1}{12} \cdot 1000 \tag{2.6}$$

For the soluble fermentation products, the expected conversion pathways were assumed (see Table 2.10). The resulting balance allowed an estimation of how much of the carbon introduced with the substrate could be recovered in the measured products.

Table 2.10: Assumed carbon flow from substrate compounds to observed products for carbon balancing.

Substrate	Observed / Assumed Products
2,3-Butanediol	2-Butanone, 2-Butanol, Acetate
Methanol	Acetate
1,2-Propanediol	1-Propanol, Propionate
Ethylene glycol	Ethanol, Acetate

The carbon balance was subsequently calculated according to Equation 2.7.

$$\text{Carbon balance} = \frac{\sum_{j=1}^{n} \left(C_{\mathrm{P}_j, t_{\mathrm{end}}} - C_{\mathrm{P}_j, t_{\mathrm{start}}} \right)}{\sum_{i=1}^{m} \left(C_{\mathrm{S}_i, t_{\mathrm{start}}} - C_{\mathrm{S}_i, t_{\mathrm{end}}} \right)} \tag{2.7}$$

where:
$C_{\mathrm{P}_j, t}$ = Carbon concentration of product j at time t
$C_{\mathrm{S}_i, t}$ = Carbon concentration of substrate i at time t
m = Number of substrates
n = Number of products
t_{start} = Initial sampling time
t_{end} = Final sampling time

CHAPTER 3

Results and Evaluation

3.1 Construction of the CRISPR array plasmid

The transformation of the spacer plasmids into *E. coli* was verified by colony PCR and agarose gel electrophoresis. For spacer 2 (see Figure 3.1), faint bands were observed near the expected size (364 bp), although some unspecific amplification occurred. Colonies 1, 2, and 4, which displayed the clearest bands, were sequenced, confirming correct integration of spacer 2. Colony 4 was subsequently selected for further use. In contrast, no bands of the correct size were detected for spacer 1 (see Figure 3.2), and sequencing confirmed unsuccessful integration. Consequently, spacer 1 was discarded.

The amplification of the homologous regions LHA and RHA from the genome of *A. woodii*, as well as the promoters pta (from *C. ijungdahlii*) and the promoter of the *AWO_RS05465* gene (*A. woodii*), was verified by agarose gel electrophoresis (see Figure 3.3). Successful amplification was confirmed by the presence of bands at approximately 1500 bp corresponding to LHA (1514 bp) and RHA (1443 bp), and bands at approximately 200 bp corresponding to the pta promoter (222 bp) and promoter of the *AWO_RS05465* gene (122 bp).

The next step involved the insertion of the homologous regions and the new promoters. Colony PCR and agarose gel electrophoresis revealed that only the assembly of the pta-promoter plasmid was successful. For the pta-promoter, three bands were observed, but only one band at the expected size of approximately 3.8 kbp was present, which was subsequently excised and sequenced (see Figure 3.4). This colony was then used for plasmid isolation via midiprep.

Although the promoter of the *AWO_RS05465* gene plasmid was subsequently retransformed, colony PCR using primers REY_007 and REY_008 (Appendix B) yielded bands of the expected size (2.3 kbp). Sequencing of these colonies, however, revealed a mutation in the alcohol dehydrogenase gene.

Due to uncertainty regarding whether the error occurred during PCR or sequencing, and since the pta-promoter was already successfully transformed into *A. woodii*, the decision was made to discard the promoter of the *AWO_RS05465* gene construct.

After midiprep, the isolated plasmid DNA was measured with the NanoDrop 1000 spectrophotometer (Thermo Fisher Scientific) at a concentration of 3158 ng/µL. The purity ratios were A260/A280 = 1.84 and A260/A230 = 2.09, both within the optimal range for pure DNA, indicating minimal contamination with proteins or salts. The obtained concentration was considerably higher than the amount typically required for transformation, ensuring sufficient material for all subsequent steps.

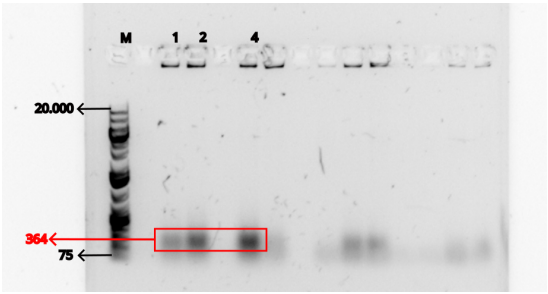


Figure 3.1: Agarose gel electrophoresis of the PCR for Spacer 2. Bands in the expected size range appear weak and unspecific, suggesting suboptimal amplification. The respective colonies were nevertheless verified by sequencing. GeneRuler 1 kb Plus DNA Ladder (Thermo Scientific) was used as a size reference (lane M).

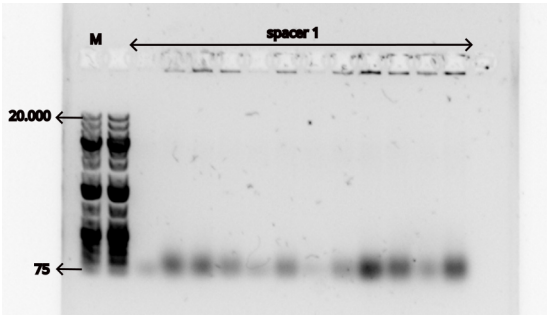


Figure 3.2: Agarose gel electrophoresis showing only primer-dimers, with no bands in the expected size range for Spacer 1. GeneRuler 1 kb Plus DNA Ladder (Thermo Scientific) was used as a size reference (lane M).

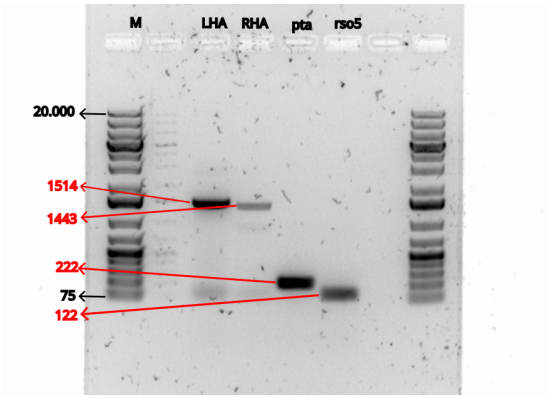


Figure 3.3: Agarose gel electrophoresis showing successful amplification of homologous regions LHA and RHA from the *A. woodii* genome, and promoters pta (from *C. ijungdahlii*) and the promoter of the *AWO_RS05465* gene (*A. woodii*). Amplified bands are highlighted in red. GeneRuler 1 kb Plus DNA Ladder (Thermo Scientific) was used as a size reference (lane M).

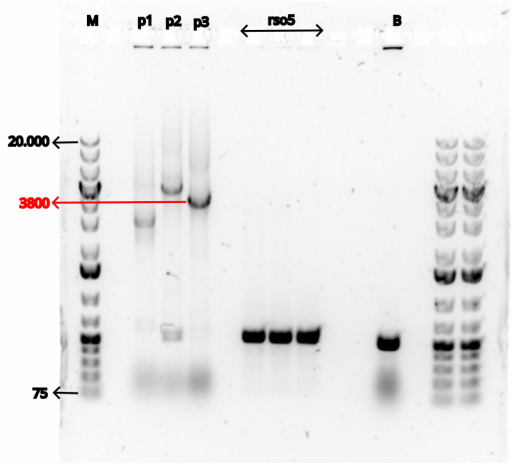


Figure 3.4: Agarose gel electrophoresis of colony PCR products. Lanes 2 and 3 show E. coli colonies containing the pta promoter, with unspecific bands. Lane 4 shows a colony with the pta promoter at the expected size. Lanes 6, 7, and 8 correspond to colonies with the RS05 promoter, which showed no bands at the expected size. Lane 10 is the negative control. GeneRuler 1 kb Plus DNA Ladder (Thermo Scientific) was used as a size reference (lane M).

3.2 Transformation of the CRISPR array plasmid into *A. woodii*

As shown in Figure 3.5, colonies 2, 4, 5, 6, 9, 10, and 12 exhibited clear bands at the expected size of 1626 base pairs in a PCR using primers KWO_139 and KWO_137 (Appendix B) with B7 High Fidelity DNA Polymerase. To verify whether any wild-type strains were still present among the colonies, an additional PCR was performed by the project supervisor using primers KWO_136 and KWO_140 (Appendix B) with B7 High Fidelity DNA Polymerase. This PCR showed no presence of the strains TU2.0 and Δ*aco1*.

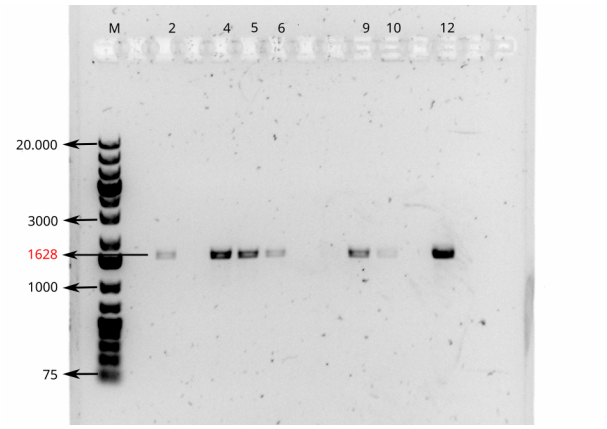


Figure 3.5: Agarose gel electrophoresis of PCR products targeting the pta promoter. Colonies 2, 4, 5, 6, 9, 10, and 12 show bands at 1600 bp, indicating successful amplification. GeneRuler 1 kb Plus DNA Ladder (Thermo Scientific) was used as a size reference (lane M).

3.3 Serum Bottle Experiments for 2-butanol Production Analysis

3.3.1 TU2.0 and Δ*aco1* under N_2/CO_2

2,3-Butanediol as Substrate

(a) $OD_{600/660}$ (b) Metabolite concentrations (HPLC)

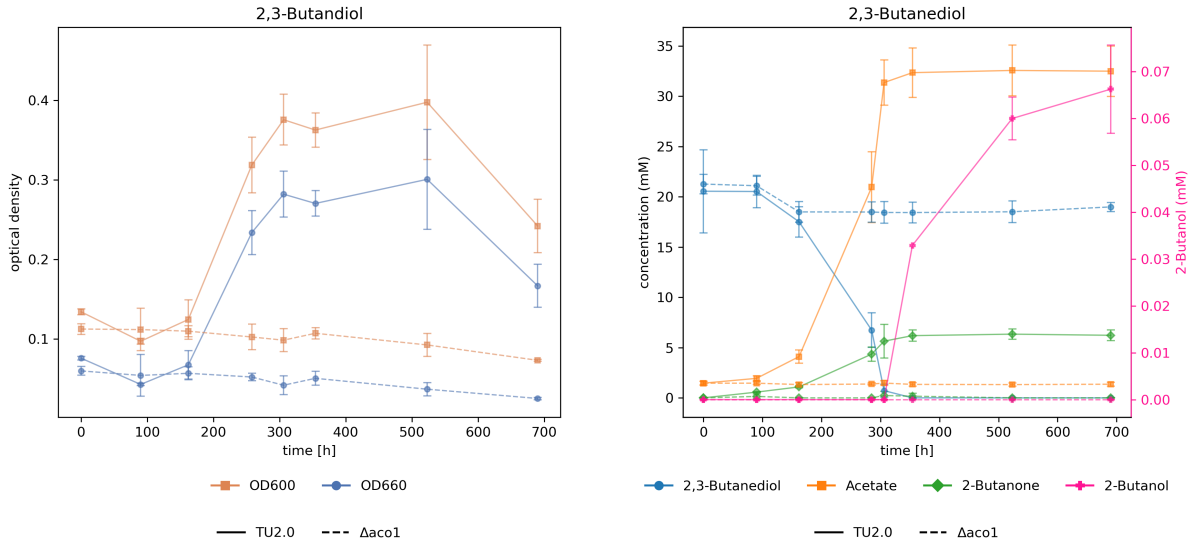


Figure 3.6: Growth curves and metabolite concentrations for *A. woodii* TU2.0 and Δ*aco1* under 2,3-butanediol in a N_2/CO_2 atmosphere using a defined phosphate-/carbonate-buffered medium. Values represent the mean ± standard deviation of three independent cultures.

As shown in Figure 3.6 (b), the wild-type strain (TU2.0) converted 2,3-butanediol to 2-butanone and acetate, consistent with the proposed metabolic pathwayIn the knockout strain, the 2,3-butanediol concentration stabilized only after approximately 162 h at around 20 mM, with the underlying reason unknown. The knockout strain did not produce 2-butanone or acetate. In the TU2.0 strain, 2-butanol was detected for the first time after 354 h of reaction time. The reaction was completed after 690 h, resulting in a final concentration of 0.066 ± 0.009 mM 2-butanol (mean ± SD, $n = 3$), which is at the detection limit and likely below the quantification limit of the HPLC method. Optical density

measurements at 600 nm and 660 nm (Figure 3.6 (a)) indicated that cell growth had ceased between approximately 523 h and 690 h, consistent with the end of the reaction period.

2,3-Butanediol and Methanol as Substrates

(a) $OD_{600/660}$ (b) Metabolite concentrations (HPLC)

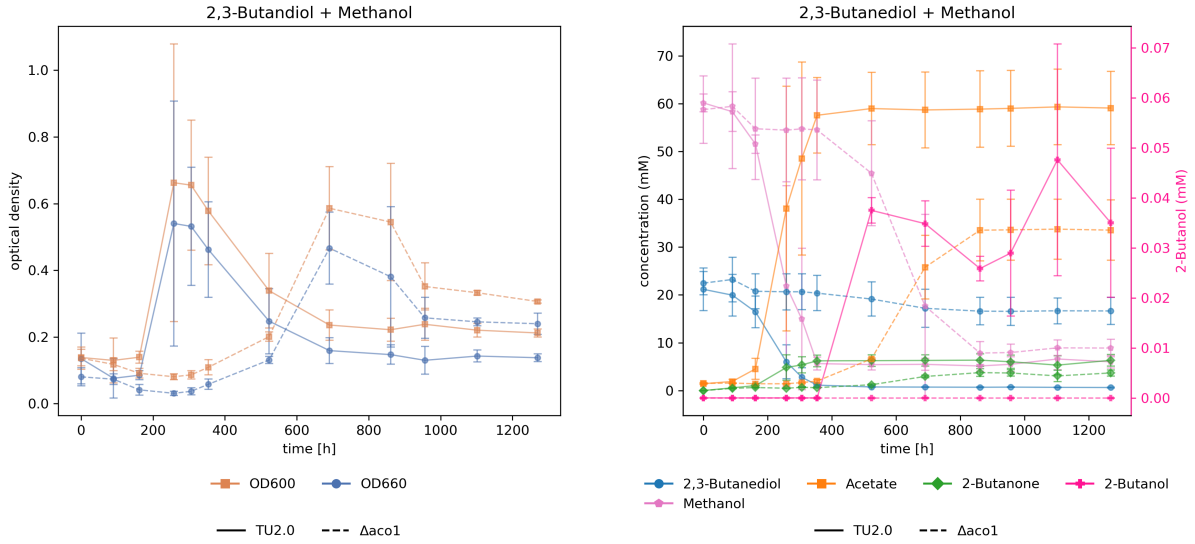


Figure 3.7: Growth curves and metabolite concentrations for *A. woodii* TU2.0 and Δ*aco1* under 2,3-butanediol and methanol in a N_2/CO_2 atmosphere using a defined phosphate-/carbonate-buffered medium. Values represent the mean ± standard deviation of three independent cultures.

As shown in Figure 3.7 (b), both 2,3-butanediol and methanol were metabolized to acetate by the TU2.0 strain. In contrast, Δ*aco1* produced only small amounts of 2-butanone (ca. 4 mM) and mainly used methanol as a carbon source. The methanol concentration in the medium was approximately 60 mM instead of the intended 50 mM.

Optical density measurements (Figure 3.7 (a)) indicated that the reaction proceeded significantly faster in the TU2.0 strain compared to Δ*aco1*. Cell growth in the TU2.0 ceased between 354 and 523 h, while Δ*aco1* reached maximum optical density only at 691 h.

Only the TU2.0 strain produced measurable amounts of 2-butanol, with a final concentration of 0.035±0.015 mM (mean ± standard deviation, n=3).

2,3-Butanediol and Ethylene glycol as Substrates

(a) $OD_{600/660}$ (b) Metabolite concentrations (HPLC)

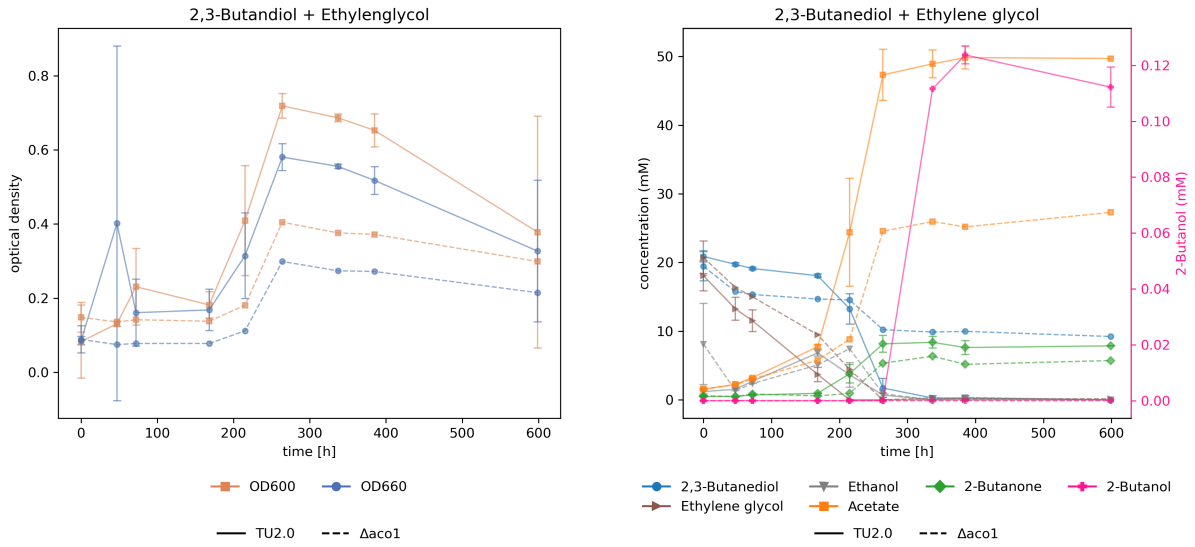


Figure 3.8: Growth curves and metabolite concentrations of A. woodii TU2.0 and Δ*aco1* grown with 2,3-butanediol and ethylen glycol in a N_2/CO_2 atmosphere using a defined phosphate-/carbonate-buffered medium. Values represent the mean ± standard deviation of two independent cultures, except for Δ*aco1*, where only one culture is shown due to oxygen contamination in the other culture.

In the TU2.0 strain, as expected, 2,3-butanediol was converted to 2-butanone and acetate. In the Δ*aco1* strain, only about 5.6 mM 2-butanone was produced.

In the TU2.0 strain, ethylene glycol was metabolized to ethanol, which subsequently served as a C_2 source and was further converted to acetate. In the Δ*aco1* strain, ethylene glycol was also metabolized to ethanol, which was subsequently converted to acetate. Notably, one serum bottle of the Δ*aco1* cultures was contaminated with oxygen, and an outlier in the ethanol concentration was observed at the beginning of the reaction due to ethanol disinfection of the serum bottle prior to sampling.

Only the TU2.0 strain produced measurable amounts of 2-butanol, with a final concentration of 0.112 ± 0.007 mM (mean ± standard deviation, n=2) (Figure 3.8 (b)).

An outlier in the OD_{660} measurement of the TU2.0 strain was observed at 46 h of reaction time. In both the TU2.0 and the Δ*aco1* knockout strain, cell growth started between 72 h and 168 h and ceased between 337 h and 385 h (Figure 3.8 (a)).

2,3-Butanediol and 1,2-Propanediol as Substrates

(a) $OD_{600/660}$ (b) Metabolite concentrations (HPLC)

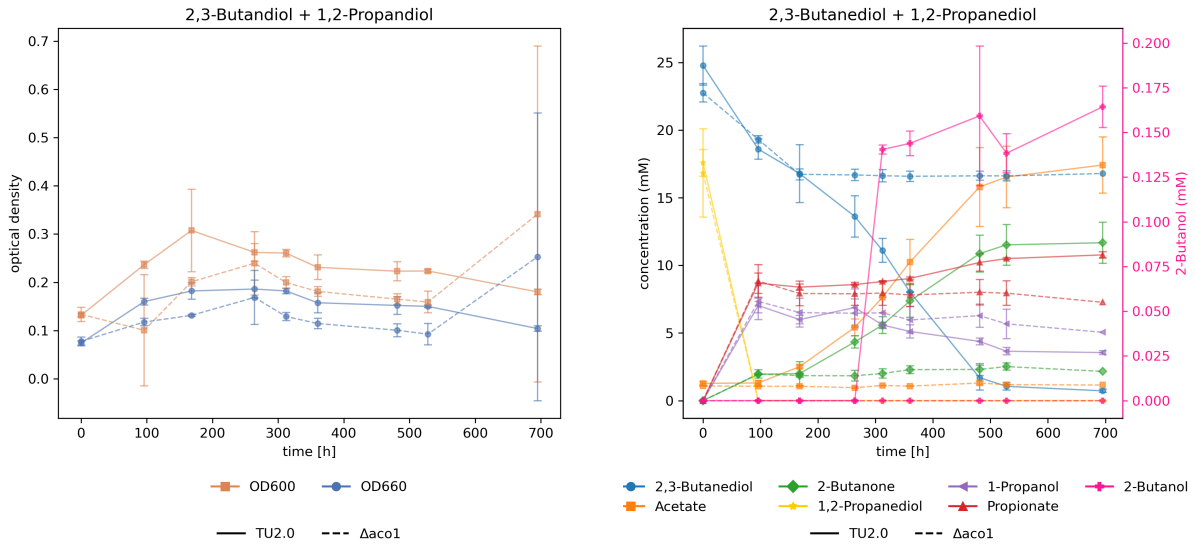


Figure 3.9: Growth curves and metabolite concentrations for *A. woodii* TU2.0 and Δ*aco1* under 2,3-butanediol and 1,2-propanediol in a N_2/CO_2 atmosphere using a defined phosphate-/carbonate-buffered medium. Values represent the mean ± standard deviation of two independent cultures.

In the TU2.0 strain, 2,3-butanediol was converted to 2-butanone and acetate, as observed in the previous experiments. For 1,2-propanediol, both strains metabolized the substrate as expected, yielding 1-propanol and propionate in approximately equal amounts via propanal as an intermediate. Propanal itself was not detected in either the TU2.0 or the Δ*aco1* strain.

As expected, the production of 2-butanol was higher than in the experiments with the other substrates, with a final concentration of 0.164 ± 0.008 mM (mean ± standard deviation, n=2) (Figure 3.9 (b)).

The $OD_{600/660}$ measurements did not reveal clear trends or strain-specific differences in cell growth for this experiment Figure 3.9 (a)).

3.3.2 TU2.0_Ppta and Δ*aco1*_Ppta under N_2/CO_2

2,3-Butanediol as Substrate

(a) $OD_{600/660}$ (b) Metabolite concentrations (HPLC)

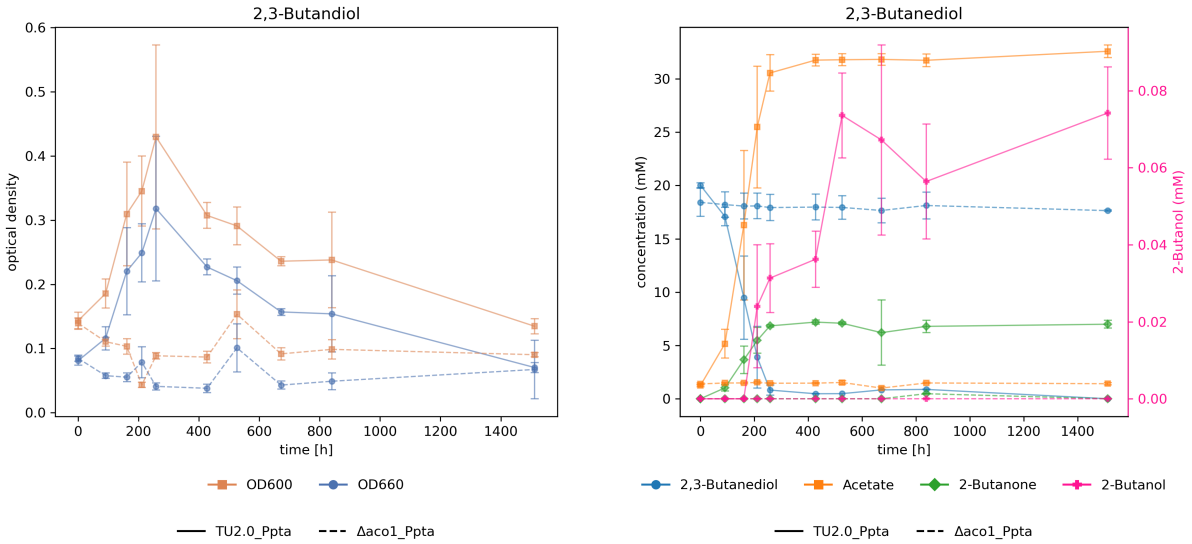


Figure 3.10: Growth curves and metabolite concentrations for *A. woodii* TU2.0_Ppta and Δ*aco1*_Ppta under 2,3-butanediol in a N_2/CO_2 atmosphere using a defined phosphate-/carbonate-buffered medium. Values represent the mean ± standard deviation of three independent cultures.

For the Ppta strains, the metabolic patterns for 2,3-butanediol were similar to those of the corresponding control strains, with no observable differences in substrate consumption or product formation, including 2-butanol (final concentration approximately 0.07 mM; Figure 3.6 and 3.10 (a) and (b)).

2,3-Butanediol and Methanol as Substrates

(a) $OD_{600/660}$ (b) Metabolite concentrations (HPLC)

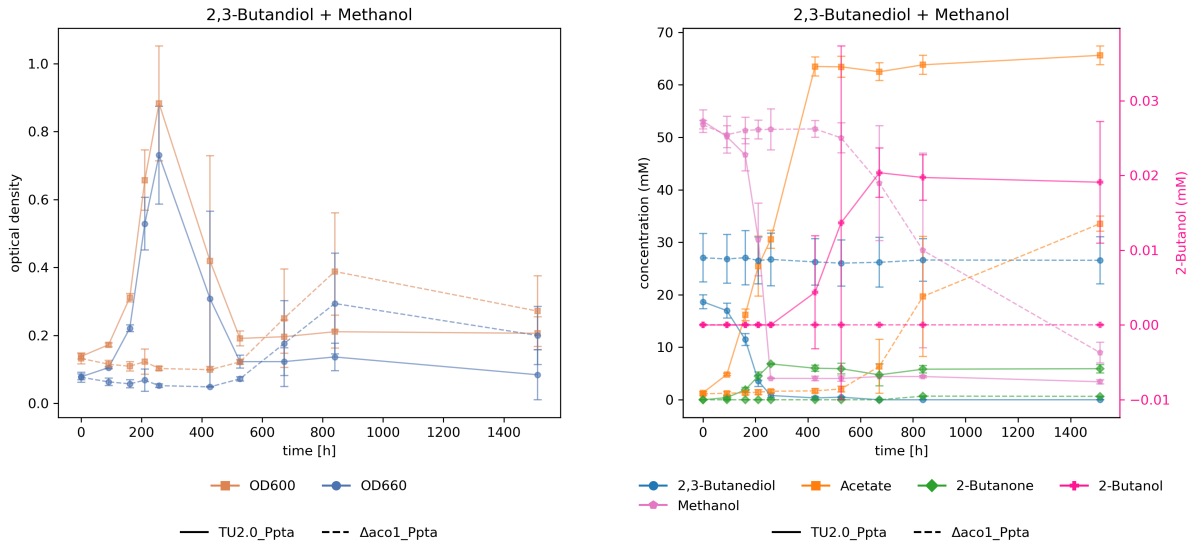


Figure 3.11: Growth curves and metabolite concentrations for *A. woodii* TU2.0_Ppta and Δ*aco1*_Ppta under 2,3-butanediol and methanol in a N_2/CO_2 atmosphere using a defined phosphate-/carbonate-buffered medium. Values represent the mean ± standard deviation of three independent cultures.

Similarly, for 2,3-butanediol and methanol, the pta promoter had no effect on the reduction of 2,3-butanediol to 2-butanol (Figure 3.11 (a) and (b)).

3.3.3 TU2.0_Ppta under H_2

2,3-Butanediol as Substrate

(a) $OD_{600/660}$ (b) Metabolite concentrations (HPLC)

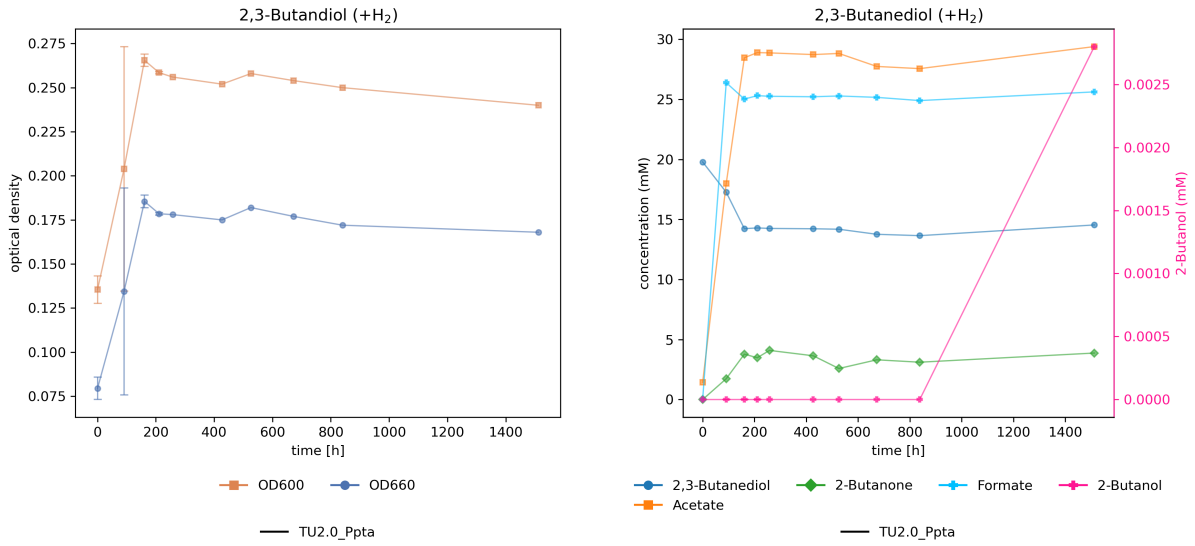


Figure 3.12: Growth curves and metabolite concentrations for *A. woodii* TU2.0_Ppta under 2,3-butanediol in a H_2 atmosphere using a defined phosphate-/carbonate-buffered medium. Single measurement from one culture; other replicates were excluded due to oxygen contamination.

Minimal reduction of 2,3-butanediol to 2-butanone was observed; however, some 2-butanol was still produced. Substantial amounts of acetate and formate (see Discussion) were formed compared to previous experiments conducted under N_2/CO_2 conditions (Figures 3.12 (a) and (b)).

A single late measurement at 1512 h showed a low 2-butanol concentration (0.003 mmol). Since no product formation had been detected for several hundred hours beforehand and the signal originated from only one replicate, this value may represent an outlier, potentially caused by analytical noise or minor handling variability.

2,3-Butanediol and Methanol as Substrates

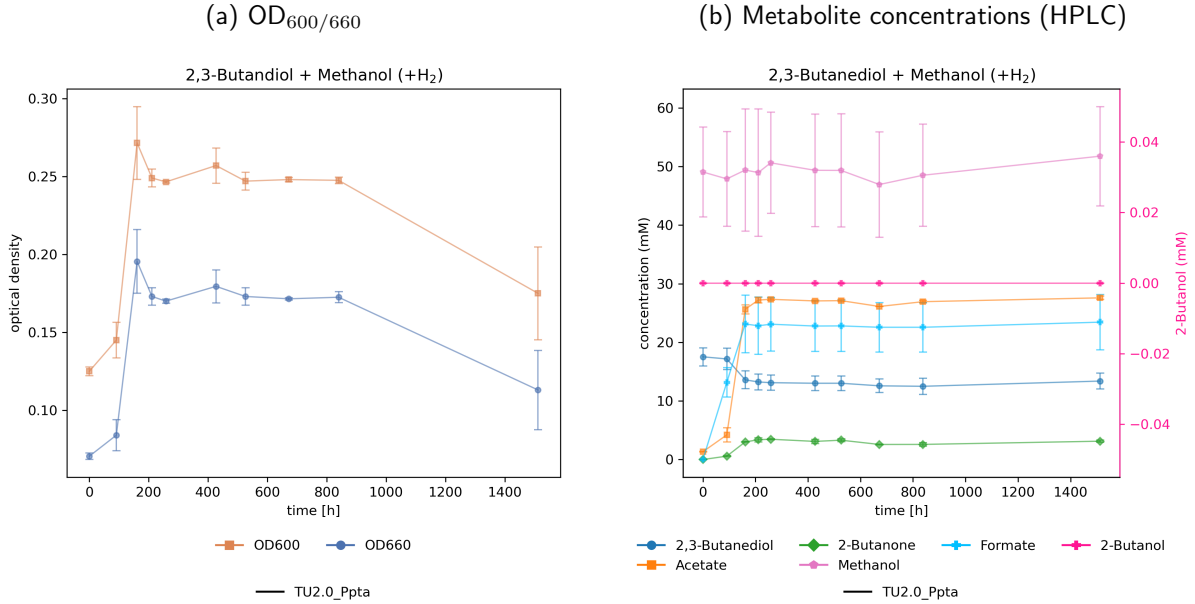


Figure 3.13: Growth curves and metabolite concentrations for *A. woodii* TU2.0_Ppta under 2,3-butanediol and methanol in a H_2 atmosphere using a defined phosphate-/carbonate-buffered medium. Single measurement from one culture; other replicates were excluded due to oxygen contamination.

The observed behavior, as illustrated in Figure 3.13 (a) and (b), was analogous to that described for 2,3-butanediol under H_2 (Section 3.3.3).

2-Butanone and 1,2-Propanediol as Substrates

(a) $OD_{600/660}$ (b) Metabolite concentrations (HPLC)

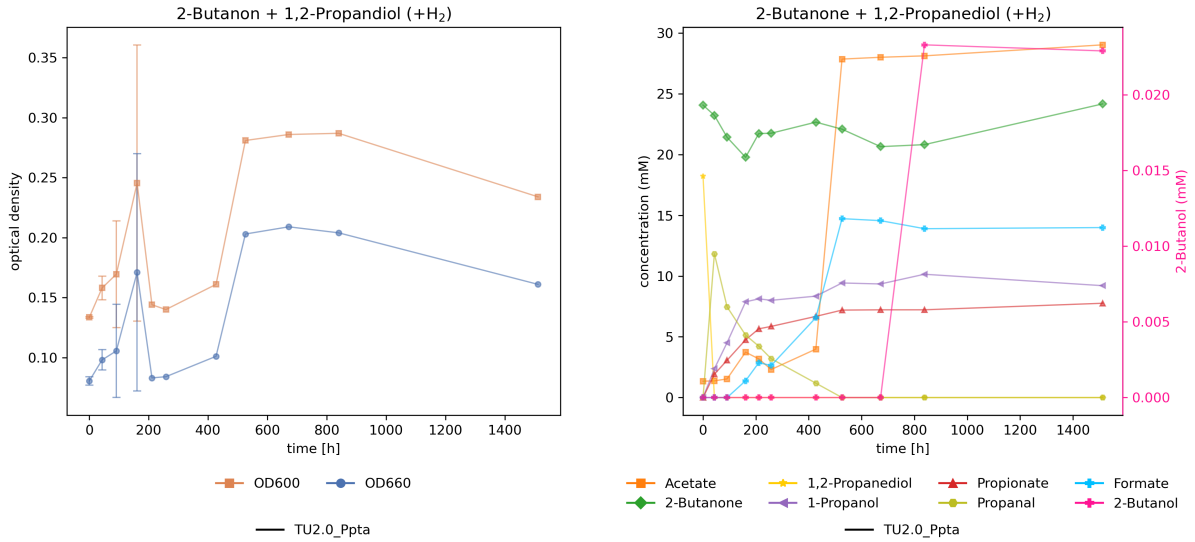


Figure 3.14: Growth curves and metabolite concentrations for *A. woodii* TU2.0_Ppta under 2-butanone and 1,2-propanediol in a H_2 atmosphere using a defined phosphate-/carbonate-buffered medium. Single measurement from one culture; other replicates were excluded due to oxygen contamination.

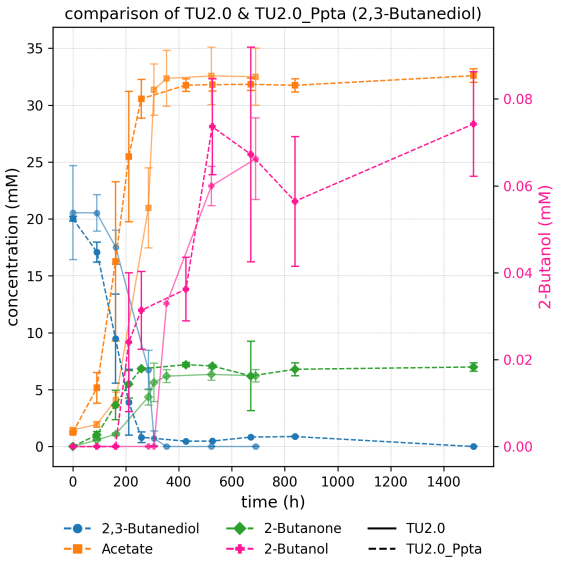
Similar behavior to the other experiments was observed. However, the reduction of 1,2-propanediol to 1-propanol and propionate proceeded very slowly, with the intermediate propanal detected for approximately 427 hours before complete conversion (Figures 3.14 (a) and (b)). One sample was excluded from analysis due to oxygen contamination.

3.3.4 Comparison of Strain Performance on 2,3-Butanediol and 2,3-Butanediol and Methanol

A direct comparison between TU2.0, TU2.0_Ppta, and Δ*aco1* is only possible for 2,3-butanediol and 2,3-butanediol with methanol, since these were the only substrates included for all four strains in the experimental design.

Figure 3.15 (a) and (b) shows the course of the enzymatic degradation of 2,3-butanediol and 2,3-butanediol with methanol as a co-substrate, respectively, comparing TU2.0 and TU2.0_Ppta. Both profiles are nearly identical, indicating that the alternative pta promoter has no significant effect on the reduction of 2-butanone to 2-butanol.

(a) 2,3-butanediol



(b) 2,3-butanediol and methanol

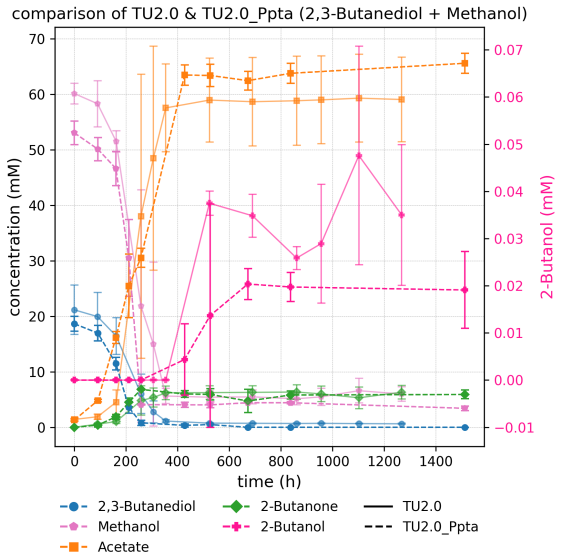
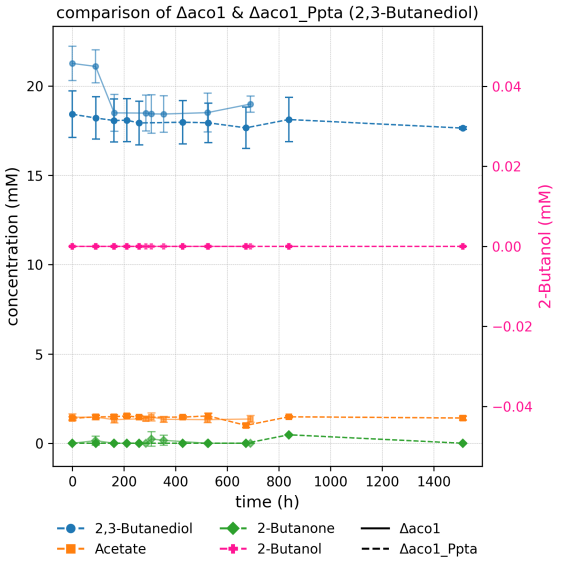


Figure 3.15: Comparison of metabolite production between *A. woodii* TU2.0 and TU2.0_Ppta, analyzed by HPLC under (a) 2,3-butanediol and (b) 2,3-butanediol + methanol in a N_2/CO_2 atmosphere using a defined phosphate-/carbonate-buffered medium. Values represent the mean ± standard deviation of three biological replicates.

Figure 3.16 (a) and (b) illustrates the enzymatic degradation profiles for the Δ*aco1* strains under the same conditions. Similarly, the data show no significant difference between the strains with and without the pta promoter, confirming that the promoter strength does not influence the reduction process in the Δ*aco1* background.

(a) 2,3-butanediol



(b) 2,3-butanediol and methanol

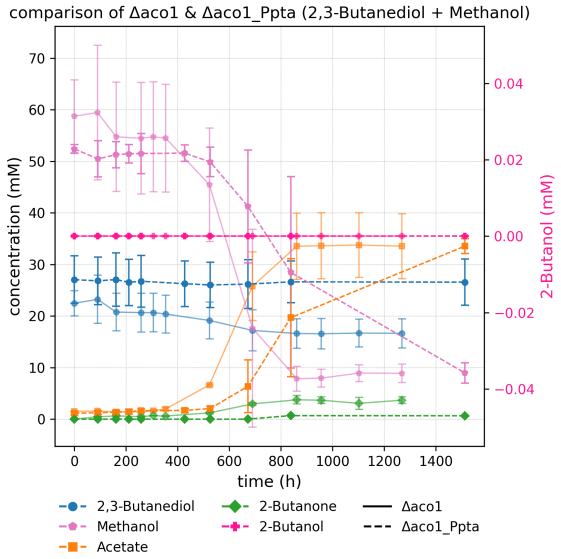


Figure 3.16: Comparison of metabolite production between *A. woodii* Δ*aco1* and Δ*aco1*_Ppta, analyzed by HPLC under (a) 2,3-butanediol and (b) 2,3-butanediol + methanol in a N_2/CO_2 atmosphere using a defined phosphate-/carbonate-buffered medium. Values represent the mean ± standard deviation of two biological replicates.

3.3.5 Carbon Recovery and Mass Balance

Figure 3.17 shows the total carbon balance of all experiments. The red dashed line at 1.0 represents the ideal carbon balance, i.e., the condition in which all carbon entering the reaction is recovered in the measured products. Experiments 4 to 10 closely matched this ideal. In contrast, experiments 1 to 3 exhibited carbon recoveries above the ideal value, whereas experiments 11 to 13 showed carbon deficits. The reasons for these deviations are discussed in Section 4.3, with further details on the high values provided in Section 4.4.

No carbon balance was determined for 2,3-butanediol with the Δ*aco1* (see Figure 3.6 (b)) and Δ*aco1*_Ppta (see Figure 3.10 (b)) strains, as 2,3-butanediol was not metabolized to acetate and 2-butanone in these strains.

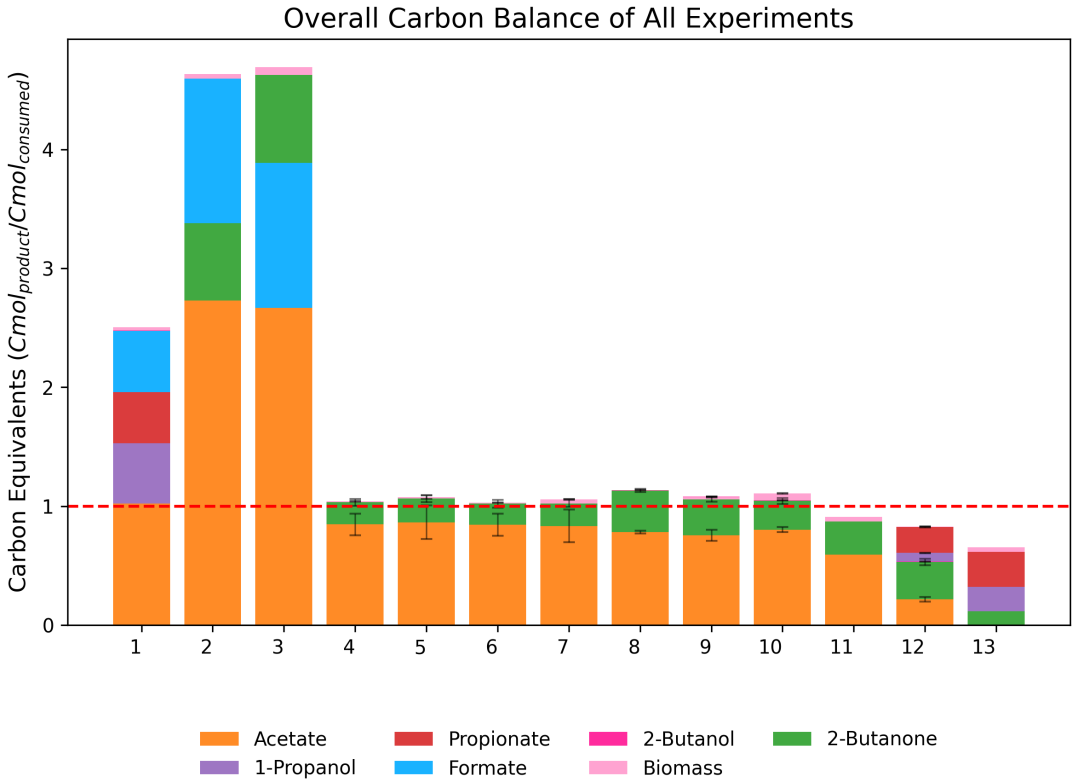


Figure 3.17: Total carbon balance of all experiments. Bars are numbered as follows: 1) 2-butanone + 1,2-propanediol (TU2.0_Ppta under H_2), 2) 2,3-butanediol + MeOH (TU2.0_Ppta under H_2), 3) 2,3-butanediol (TU2.0_Ppta under H_2), 4) 2,3-butanediol + MeOH (TU2.0_Ppta), 5) 2,3-butanediol + MeOH (Δ*aco1*_Ppta), 6) 2,3-butanediol + MeOH (TU2.0), 7) 2,3-butanediol + MeOH (Δ*aco1*), 8) 2,3-butanediol (TU2.0_Ppta), 9) 2,3-butanediol (TU2.0), 10) 2,3-butanediol + ethylene glycol (TU2.0), 11) 2,3-butanediol + ethylene glycol (Δ*aco1*), 12) 2,3-butanediol + 1,2-propanediol (TU2.0), 13) 2,3-butanediol + 1,2-propanediol (Δ*aco1*). The dashed red line indicates the theoretical maximum carbon recovery (value = 1) for reference.

CHAPTER 4

Discussion

4.1 Promoter Exchange of ADH4 in *A. woodii*

One objective of this study was to replace the promoter of *adh4* with a alternative promoter (PTA or the promoter of the *AWO_RS05465* gene) to enhance the production of 2-butanol. For this purpose, two different CRISPR spacers were provided as a backup strategy.

Of the two spacers, only Spacer 2 was successfully utilized; Spacer 1 could not be assembled into the plasmid despite multiple attempts. A plausible explanation is that Spacer 1 forms unfavorable secondary structures in the gRNA (e.g., hairpins), which can interfere with primer annealing or plasmid assembly efficiency and thereby prevent its functional evaluation [Ohshima and Wells, 1997].

The PTA promoter was successfully transformed into *A. woodii*. The incorporation of the promoter of the *AWO_RS05465* gene was not performed, as a mutation in the *adh4* sequence was identified in the plasmid upon sequencing.

It is more likely that this mutation occurred during PCR amplification, as sequencing errors in modern methods are relatively rare [Crossley et al., 2020, McInerney et al., 2014]. To avoid potential sources of error, transformation with the promoter of the *AWO_RS05465* gene was therefore omitted.

Analysis of 2-butanol production showed no increase with the introduced PTA promoter. This suggests that the limitation is not in the expression of ADH4 but is likely determined by other factors in the metabolism. For instance, the redox balance ($NADH/NAD^+$) could limit the reduction steps, or the rate at which carbon flows through the WLP may restrict the availability of precursors for 2-butanol synthesis.

Overall, it is evident that an alternative promoter alone is insufficient to increase 2-butanol production.

4.2 Effect of 1,2-Propanediol on 2-Butanol Formation

Within the scope of this work, it was investigated whether 1,2-propanediol as a co-substrate influences the reduction of 2-butanone to 2-butanol in *A. woodii* via PduQ. The results demonstrated that the addition of 1,2-propanediol indeed promotes 2-butanol formation.

Acetobacterium woodii is known to metabolize 1,2-propanediol independently of acetogenesis, forming propionaldehyde, which is oxidized to propionyl-CoA with concomitant NADH formation, while NAD^+ is regenerated by reduction of propionaldehyde to propanol [Schuchmann et al., 2015]. This metabolism is associated with a gene cluster encoding bacterial microcompartment (BMC) proteins, including an alcohol dehydrogenase homologous to PduQ, which facilitates intracellular $NADH/NAD^+$ recycling.

Although 1,2-propanediol metabolism in *A. woodii* has been less extensively studied, it has been shown that *A. woodii* can grow on 1,2-propanediol [Chowdhury et al., 2020], and that deletion of

the *adh4* gene reduces propanol formation [Chowdhury et al., 2021], indicating a functional pathway for 1,2-propanediol utilization. In *S. enterica* [Cheng et al., 2012], the alcohol dehydrogenase PduQ plays a central role in NADH/NAD^+ recycling within a Pdu-type BMC, thereby maintaining cofactor balance for the dehydrogenase reactions.

A possible explanation in *A. woodii* is that during 1,2-propanediol metabolism, both a carboxylic acid (propionic acid) and an alcohol (propanol) are produced, enabling regeneration of NAD^+ from NADH. In contrast, during 2,3-butanediol metabolism, the dehydrogenation step yields a ketone rather than an aldehyde. While ketones can be reduced to alcohols, they cannot be oxidized, so NAD^+ regeneration is not possible. If 1,2-propanediol and 2,3-butanediol are present simultaneously, NAD^+ regeneration via 1,2-propanediol metabolism could theoretically enable limited conversion of 2,3-butanediol to 2-butanol. This suggests that the effect of 1,2-propanediol on 2-butanol formation in *A. woodii* is mediated through cofactor regeneration, potentially involving Adh4.

These results support the hypothesis that 1,2-propanediol as a co-substrate facilitates PduQ-catalyzed reduction of 2-butanone to 2-butanol.

4.3 Carbon balance of mixed-substrate fermentations

As shown in Section 3.3.5 and Figure 3.17, most of the carbon balances were close to 100 %, except for three cases measured under N_2/CO_2 conditions, which fell below full recovery: 2,3-butanediol + ethylene glycol (Δ*aco1*, 90 %), 2,3-butanediol + 1,2-propanediol (TU2.0, 82 %), and 2,3-butanediol + 1,2-propanediol (Δ*aco1*, 65%). Carbon balances under H_2 atmosphere were generally above 100 % (see section 4.4).

The missing fraction of carbon in some cases can be explained by several factors: (i) volatile intermediates, such as ethanol or propanal, which may partition into the gas phase and are not detected by HPLC (propanal, with a boiling point of 49°C, was observed to evaporate even during standard preparation), (ii) dissolved inorganic carbon (DIC), e.g., CO_2(aq) or bicarbonate, that was not quantified, (iii) general uncertainties in estimating biomass carbon via OD/CDW conversions, which may introduce a slight systematic error affecting all samples, and (iv) minor volume losses due to sampling.

4.4 Hypothesis on the Preferential Use of the Wood-Ljungdahl Pathway under H_2 Conditions

As shown in Section 3.3.5 and Figure 3.17, most carbon recoveries were close to 100 %, with the exception of three cases under N_2/CO_2 conditions that fell below full recovery. In contrast, the apparent carbon recoveries under H_2 conditions substantially exceeded the input, reaching 469 % for 2,3-butanediol (TU2.0_Ppta), 459 % for 2,3-butanediol + methanol (TU2.0_Ppta), and 250 % for 2-butanone + 1,2-propanediol (TU2.0_Ppta).

These unexpectedly high values likely result from the preferential utilization of the WLP by *A. woodii* under H_2-rich conditions. The WLP enables direct incorporation of carbonate from the medium as a carbon source [Ragsdale and Pierce, 2008] and provides an energetically favorable route for acetate production, as acetate formation from H_2 and CO_2 is coupled to net ATP synthesis [Schoberth, 1977]. This pathway serves as the primary metabolic route for this organism under autotrophic conditions [Bertsch and Müller, 2015]. Consequently, alternative substrates such as 2,3-butanediol or 1,2-propanediol may be minimally metabolized, potentially due to enzymatic inhibition or the high redox potential associated with H_2 oxidation, which could contribute to the apparent overestimation of carbon recovery in the measurements.

4.5 Challenges in HPLC quantification of 2-butanol

As shown in Section 3.3 and Figure 3.6 to 3.14, the irregular "zig-zag" pattern observed for the 2-butanol curves can be attributed to the very low amounts of product formed, which were barely recognized as 2-butanol peaks by Chromeleon. Additionally, a neighboring peak originating from a previous sample, likely due to components in the medium, co-eluted with the 2-butanol peak. This residual compound remained in the HPLC column and appeared delayed in subsequent runs. To achieve a clean separation of 2-butanol, the HPLC runtime was shortened. Consequently, in the initial measurements the 2-butanol peaks were partially truncated by the adjacent larger peak during integration, resulting in irregular peak shapes. After the measurement time was shortened, this overlap no longer occurred.

4.6 Outliers in Optical Density Measurements

Despite thorough vortexing prior to measurement, occasional outliers in OD readings were observed, notably in Figures 3.8 and 3.10. These deviations are most likely attributable to incomplete homogenization of the culture, which can lead to transient cell clumping and locally elevated cell densities. Additionally, air bubbles or foam trapped in the culture during sampling may have caused sporadic light scattering, resulting in artificially high readings. Instrumental factors, such as minor variations in the light path or condensation on the cuvette, may have further contributed to measurement variability. Finally, short-term sedimentation of cells between vortexing and measurement could have exacerbated these deviations.

To reduce such outliers in future experiments, repeated measurements, careful removal of air bubbles, and thorough homogenization immediately prior to sampling are recommended.

CHAPTER 5

Outlook

The results of this work suggest that the expression level of ADH4 is not the main limitation for 2-butanol production in *A. woodii*. Instead, the availability of reducing equivalents (NADH/NAD^+ balance) seems to play a more critical role.

Future work should therefore focus on strategies to increase NADH availability, such as modifying competing pathways, testing cofactor engineering approaches, or optimizing cultivation conditions that favor a more reduced cellular state. Additionally, redirecting flux within the WLP could help provide the necessary redox power for efficient butanol formation.

Overall, this highlights that further improvements in 2-butanol production will require metabolic engineering beyond promoter strength, with special attention to redox balance and energy metabolism.

List of Figures

1.1 Schematic representation of the WLP in *A. woodii*, showing the methyl and carbonyl branches that come together in the formation of acetyl-CoA. Adapted from Klara Wögerbauer. . . . 2

1.2 Schematic representation of 2,3-butanediol metabolism in *A. woodii*. 2,3-butanediol is oxidized by the PduCDE complex to 2-butanone (MEK), which can be reduced to 2-butanol by PduQ (ADH4). Simultaneously, 2,3-butanediol can be converted to acetoin by budC. Acetoin is degraded by Aco1 to one molecule of acetaldehyde and one molecule of acetyl-CoA; the acetaldehyde is subsequently oxidized to a second molecule of acetyl-CoA, with one acetyl-CoA molecule converted to acetate with concomitant ATP formation. Adapted from Klara Wögerbauer. . . . 3

1.3 Schematic overview of the endogenous Type I-B CRISPR/Cas system mediated promoter replacement in *A. woodii*. A synthetic CRISPR array provides a crRNA that guides the Cascade complex to the target site next to a PAM sequence. Cas3 is then recruited and introduces a double-strand break in the genomic DNA. Homologous recombination with a donor DNA template containing the new promoter flanked by left and right homology arms (LHA and RHA) enables the integration of the modified sequence. (Adapted from a BioRender template by Esmée Dragt (biorender.com).) . . . 4

1.4 Schematic overview of the Golden Gate cloning process. (1) Linearized plasmid and DNA inserts with designed overhangs. (2) Complementary overhangs anneal. (3) T4 DNA ligase seals the nicks, yielding the final assembled plasmid. (Adapted from a BioRender template by Samara Ona (biorender.com).) . . . 4

2.1 Linear regression of refractive index (RI) peak areas against known 2-butanone concentrations. The resulting calibration equation allows conversion of concentrations determined from UV280 spectra into expected RI peak areas. . . . 13

2.2 Linear regression of the calibration curve for 1-propanol, relating RI peak areas to known concentrations. The resulting regression equation enables conversion of calculated peak areas into concentrations. . . . 13

3.1 Agarose gel electrophoresis of the PCR for Spacer 2. Bands in the expected size range appear weak and unspecific, suggesting suboptimal amplification. The respective colonies were nevertheless verified by sequencing. GeneRuler 1 kb Plus DNA Ladder (Thermo Scientific) was used as a size reference (lane M). . . . 18

3.2 Agarose gel electrophoresis showing only primer-dimers, with no bands in the expected size range for Spacer 1. GeneRuler 1 kb Plus DNA Ladder (Thermo Scientific) was used as a size reference (lane M). . . . 18

3.3 Agarose gel electrophoresis showing successful amplification of homologous regions LHA and RHA from the *A. woodii* genome, and promoters pta (from *C. ijungdahlii*) and the promoter of the *AWO_RS05465* gene (*A. woodii*). Amplified bands are highlighted in red. GeneRuler 1 kb Plus DNA Ladder (Thermo Scientific) was used as a size reference (lane M). . . . 18

3.4 Agarose gel electrophoresis of colony PCR products. Lanes 2 and 3 show E. coli colonies containing the pta promoter, with unspecific bands. Lane 4 shows a colony with the pta promoter at the expected size. Lanes 6, 7, and 8 correspond to colonies with the RS05 promoter, which showed no bands at the expected size. Lane 10 is the negative control. GeneRuler 1 kb Plus DNA Ladder (Thermo Scientific) was used as a size reference (lane M). 18
3.5 Agarose gel electrophoresis of PCR products targeting the pta promoter. Colonies 2, 4, 5, 6, 9, 10, and 12 show bands at 1600 bp, indicating successful amplification. GeneRuler 1 kb Plus DNA Ladder (Thermo Scientific) was used as a size reference (lane M). 19
3.6 Growth curves and metabolite concentrations for *A. woodii* TU2.0 and Δ*aco1* under 2,3-butanediol in a N_2/CO_2 atmosphere using a defined phosphate-/carbonate-buffered medium. Values represent the mean ± standard deviation of three independent cultures. 19
3.7 Growth curves and metabolite concentrations for *A. woodii* TU2.0 and Δ*aco1* under 2,3-butanediol and methanol in a N_2/CO_2 atmosphere using a defined phosphate-/carbonate-buffered medium. Values represent the mean ± standard deviation of three independent cultures. 20
3.8 Growth curves and metabolite concentrations of A. woodii TU2.0 and Δ*aco1* grown with 2,3-butanediol and ethylen glycol in a N_2/CO_2 atmosphere using a defined phosphate-/carbonate-buffered medium. Values represent the mean ± standard deviation of two independent cultures, except for Δ*aco1*, where only one culture is shown due to oxygen contamination in the other culture. 21
3.9 Growth curves and metabolite concentrations for *A. woodii* TU2.0 and Δ*aco1* under 2,3-butanediol and 1,2-propanediol in a N_2/CO_2 atmosphere using a defined phosphate-/carbonate-buffered medium. Values represent the mean ± standard deviation of two independent cultures. 22
3.10 Growth curves and metabolite concentrations for *A. woodii* TU2.0_Ppta and Δ*aco1*_Ppta under 2,3-butanediol in a N_2/CO_2 atmosphere using a defined phosphate-/carbonate-buffered medium. Values represent the mean ± standard deviation of three independent cultures. 23
3.11 Growth curves and metabolite concentrations for *A. woodii* TU2.0_Ppta and Δ*aco1*_Ppta under 2,3-butanediol and methanol in a N_2/CO_2 atmosphere using a defined phosphate-/carbonate-buffered medium. Values represent the mean ± standard deviation of three independent cultures. 24
3.12 Growth curves and metabolite concentrations for *A. woodii* TU2.0_Ppta under 2,3-butanediol in a H_2 atmosphere using a defined phosphate-/carbonate-buffered medium. Single measurement from one culture; other replicates were excluded due to oxygen contamination. 24
3.13 Growth curves and metabolite concentrations for *A. woodii* TU2.0_Ppta under 2,3-butanediol and methanol in a H_2 atmosphere using a defined phosphate-/carbonate-buffered medium. Single measurement from one culture; other replicates were excluded due to oxygen contamination. 25
3.14 Growth curves and metabolite concentrations for *A. woodii* TU2.0_Ppta under 2-butanone and 1,2-propanediol in a H_2 atmosphere using a defined phosphate-/carbonate-buffered medium. Single measurement from one culture; other replicates were excluded due to oxygen contamination. 26
3.15 Comparison of metabolite production between *A. woodii* TU2.0 and TU2.0_Ppta, analyzed by HPLC under (a) 2,3-butanediol and (b) 2,3-butanediol + methanol in a N_2/CO_2 atmosphere using a defined phosphate-/carbonate-buffered medium. Values represent the mean ± standard deviation of three biological replicates. 27
3.16 Comparison of metabolite production between *A. woodii* Δ*aco1* and Δ*aco1*_Ppta, analyzed by HPLC under (a) 2,3-butanediol and (b) 2,3-butanediol + methanol in a N_2/CO_2 atmosphere using a defined phosphate-/carbonate-buffered medium. Values represent the mean ± standard deviation of two biological replicates. 27

3.17 Total carbon balance of all experiments. Bars are numbered as follows: 1) 2-butanone + 1,2-propanediol (TU2.0_Ppta under H_2), 2) 2,3-butanediol + MeOH (TU2.0_Ppta under H_2), 3) 2,3-butanediol (TU2.0_Ppta under H_2), 4) 2,3-butanediol + MeOH (TU2.0_Ppta), 5) 2,3-butanediol + MeOH (Δ*aco1*_Ppta), 6) 2,3-butanediol + MeOH (TU2.0), 7) 2,3-butanediol + MeOH (Δ*aco1*), 8) 2,3-butanediol (TU2.0_Ppta), 9) 2,3-butanediol (TU2.0), 10) 2,3-butanediol + ethylene glycol (TU2.0), 11) 2,3-butanediol + ethylene glycol (Δ*aco1*), 12) 2,3-butanediol + 1,2-propanediol (TU2.0), 13) 2,3-butanediol + 1,2-propanediol (Δ*aco1*). The dashed red line indicates the theoretical maximum carbon recovery (value = 1) for reference. 28

List of Tables

2.1 Composition of stock solutions used in all media. 7
2.2 Ingredients for 1 L of the defined growth medium 7
2.3 Composition of 1 L undefined medium for agar plates. 8
2.4 Antibiotics used for the bacterial strains 8
2.5 Composition of 1 L undefined medium 8
2.6 *A. woodii* strains used in this study. 11
2.7 Codes and details for serum bottles with strains expressing native promoter (strain, carbon source and gas phase). 11
2.8 Codes and details for serum bottles with transformed *A. woodii* strains expressing the *pta* promoter (strain, carbon source and gas phase). 12
2.9 Overview of relevant compounds used for carbon balancing. The number of carbon atoms per molecule was used to calculate mmol of carbon from measured concentrations. . . 14
2.10 Assumed carbon flow from substrate compounds to observed products for carbon balancing. 14

1 Preparation of HPLC standards. 43
2 Primers used in this study. 45

Bibliography

[Balch et al., 1977] Balch, W., Schoberth, S., Tanner, R., and Wolfe, R. (1977). Methanogenic bacteria: characterization of an unusual anaerobic group of bacteria. *International Journal of Systematic Bacteriology*, 27(4):355–361.

[Bertsch and Müller, 2015] Bertsch, J. and Müller, V. (2015). Co metabolism in the acetogen acetobacterium woodii. *Applied and Environmental Microbiology*, 81(17):5949–5956.

[Boudry et al., 2015] Boudry, P., Semenova, E., Monot, M., Datsenko, K. A., Lopatina, A., Sekulovic, O., Ospina-Bedoya, M., Fortier, L.-C., Severinov, K., Dupuy, B., and Soutourina, O. (2015). Function of the crispr-cas system of the human pathogen clostridium difficile. *mBio*, 6(5):10.1128/mbio.01112–15.

[Cheng et al., 2012] Cheng, S., Fan, C., Sinha, S., and Bobik, T. A. (2012). The pduq enzyme is an alcohol dehydrogenase used to recycle nad+ internally within the pdu microcompartment of salmonella enterica. *PLOS ONE*, 7(10):1–11.

[Chowdhury et al., 2020] Chowdhury, N. P., Alberti, L., Linder, M., and Müller, V. (2020). Exploring bacterial microcompartments in the acetogenic bacterium acetobacterium woodii. *Frontiers in Microbiology*, Volume 11 - 2020.

[Chowdhury et al., 2021] Chowdhury, N. P., Moon, J., and Müller, V. (2021). Adh4, an alcohol dehydrogenase controls alcohol formation within bacterial microcompartments in the acetogenic bacterium acetobacterium woodii. *Environmental Microbiology*, 23(1):499–511.

[Crossley et al., 2020] Crossley, B. M., Bai, J., Glaser, A., Maes, R., Porter, E., Killian, M. L., Clement, T., and Toohey-Kurth, K. (2020). Guidelines for sanger sequencing and molecular assay monitoring. *Journal of Veterinary Diagnostic Investigation*, 32(6):767–775. PMID: 32070230.

[Dangel et al., 1987] Dangel, W., Schulz, H., Diekert, G., König, H., and Fuchs, G. (1987). Occurrence of corrinoid-containing membrane proteins in anaerobic bacteria. *Archives of Microbiology*, 148(1):52–56.

[Debabov, 2021] Debabov, V. G. (2021). Acetogens: Biochemistry, bioenergetics, genetics, and biotechnological potential. *Microbiology*, 90(3):273–297.

[Diekert, 1992] Diekert, G. (1992). Acetogenic bacteria. In Balows, A., Trüper, H., Dworkin, M., Harder, W., and Schleifer, K.-H., editors, *The Prokaryotes*, pages 517–533. Springer-Verlag, New York.

[Drake, 1994] Drake, H. L. (1994). *Acetogenesis, Acetogenic Bacteria, and the Acetyl-CoA "Wood/Ljungdahl" Pathway: Past and Current Perspectives*, pages 3–60. Springer US, Boston, MA.

[Engler et al., 2008] Engler, C., Kandzia, R., and Marillonnet, S. (2008). A one pot, one step, precision cloning method with high throughput capability. *PLOS ONE*, 3(11):1–7.

[Engler et al., 2014] Engler, C., Youles, M., Gruetzner, R., Ehnert, T.-M., Werner, S., Jones, J. D. G., Patron, N. J., and Marillonnet, S. (2014). A golden gate modular cloning toolbox for plants. *ACS Synthetic Biology*, 3(11):839–843.

[Fuchs, 1986] Fuchs, G. (1986). Co2 fixation in acetogenic bacteria: variations on a theme. *FEMS Microbiology Reviews*, 2(3):181–213.

[Godley et al., 1990] Godley, A. R., Linnett, P. E., and Robinson, J. P. (1990). The effect of carbon dioxide on the growth kinetics of fructose-limited chemostat cultures of acetobacterium woodii dsm 1030. *Archives of Microbiology*, 154(1):5–11.

[Harvey and Meylemans, 2011] Harvey, B. G. and Meylemans, H. A. (2011). The role of butanol in the development of sustainable fuel technologies. *Journal of Chemical Technology & Biotechnology*, 86(1):2–9.

[Hess et al., 2015] Hess, V., Oyrik, O., Trifunović, D., and Müller, V. (2015). 2, 3-butanediol metabolism in the acetogen acetobacterium woodii. *Applied and Environmental Microbiology*, 81(14):4711–4719.

[Kim et al., 2019] Kim, J. et al. (2019). Microbial production of 2,3-butanediol for industrial applications. *Journal of Industrial Microbiology & Biotechnology*.

[Ljungdhal, 1986] Ljungdhal, L. G. (1986). The autotrophic pathway of acetate synthesis in acetogenic bacteria. *Annual Review of Microbiology*, 40(Volume 40, 1986):415–450.

[Maikova et al., 2019] Maikova, A., Kreis, V., Boutserin, A., Severinov, K., and Soutourina, O. (2019). Using an endogenous crispr-cas system for genome editing in the human pathogen clostridium difficile. *Applied and Environmental Microbiology*, 85(20):e01416–19.

[Martin, 2020] Martin, W. F. (2020). Older than genes: The acetyl coa pathway and origins. *Frontiers in Microbiology*, 11:817.

[McInerney et al., 2014] McInerney, P., Adams, P., and Hadi, M. Z. (2014). Error rate comparison during polymerase chain reaction by dna polymerase. *Molecular Biology International*, 2014(1):287430.

[Moon et al., 2019] Moon, S. B., Kim, D. Y., Ko, J.-H., and Kim, Y.-S. (2019). Recent advances in the crispr genome editing tool set. *Experimental & Molecular Medicine*, 51(11):1–11.

[Mulepati and Bailey, 2013] Mulepati, S. and Bailey, S. (2013). In vitro reconstitution of an escherichia coli rna-guided immune system reveals unidirectional, atp-dependent degradation of dna target*. *Journal of Biological Chemistry*, 288(31):22184–22192.

[Neuendorf et al., 2021] Neuendorf, C. S., Vignolle, G. A., Derntl, C., Tomin, T., Novak, K., Mach, R. L., Birner-Grünberger, R., and Pflügl, S. (2021). A quantitative metabolic analysis reveals acetobacterium woodii as a flexible and robust host for formate-based bioproduction. *Metabolic Engineering*, 68:68–85.

[Ohshima and Wells, 1997] Ohshima, K. and Wells, R. D. (1997). Hairpin formation during dna synthesis primer realignmentin vitro in triplet repeat sequences from human hereditary disease genes*. *Journal of Biological Chemistry*, 272(27):16798–16806.

[Oppermann et al., 1991] Oppermann, F. B., Schmidt, B., and Steinbüchel, A. (1991). Purification and characterization of acetoin:2,6-dichlorophenolindophenol oxidoreductase, dihydrolipoamide dehydrogenase, and dihydrolipoamide acetyltransferase of the pelobacter carbinolicus acetoin dehydrogenase enzyme system. *Journal of Bacteriology*, 173(2):757–767.

[Patron et al., 2015] Patron, N. J., Orzaez, D., Marillonnet, S., Warzecha, H., Matthewman, C., Youles, M., Raitskin, O., Leveau, A., Farré, G., Rogers, C., Smith, A., Hibberd, J., Webb, A. A. R., Locke, J., Schornack, S., Ajioka, J., Baulcombe, D. C., Zipfel, C., Kamoun, S., Jones, J. D. G., Kuhn, H., Robatzek, S., Van Esse, H. P., Sanders, D., Oldroyd, G., Martin, C., Field, R., O'Connor, S., Fox, S., Wulff, B., Miller, B., Breakspear, A., Radhakrishnan, G., Delaux, P.-M., Loqué, D., Granell, A., Tissier, A., Shih, P., Brutnell, T. P., Quick, W. P., Rischer, H., Fraser, P. D.,

Aharoni, A., Raines, C., South, P. F., Ané, J.-M., Hamberger, B. R., Langdale, J., Stougaard, J., Bouwmeester, H., Udvardi, M., Murray, J. A. H., Ntoukakis, V., Schäfer, P., Denby, K., Edwards, K. J., Osbourn, A., and Haseloff, J. (2015). Standards for plant synthetic biology: a common syntax for exchange of dna parts. *New Phytologist*, 208(1):13–19.

[Poulalier-Delavelle et al., 2023] Poulalier-Delavelle, M., Baker, J. P., Millard, J., Winzer, K., and Minton, N. P. (2023). Endogenous crispr/cas systems for genome engineering in the acetogens acetobacterium woodii and clostridium autoethanogenum. *Frontiers in Bioengineering and Biotechnology*, Volume 11 - 2023.

[Ragsdale, 1991] Ragsdale, S. W. (1991). Enzymology of the acetyl-coa pathway of co2 fixation. *Critical reviews in biochemistry and molecular biology*, 26(3-4):261–300.

[Ragsdale and Pierce, 2008] Ragsdale, S. W. and Pierce, E. (2008). Acetogenesis and the wood-ljungdahl pathway of co(2) fixation. *Biochimica et Biophysica Acta (BBA) - Proteins and Proteomics*, 1784(12):1873–1898.

[Russmayer et al., 2019] Russmayer, H., Marx, H., and Sauer, M. (2019). Microbial 2-butanol production with lactobacillus diolivorans. *Biotechnology for Biofuels*, 12(1):262.

[Schoberth, 1977] Schoberth, S. (1977). Acetic acid from h2 and co2. *Archives of Microbiology*, 114(2):143–148.

[Schoelmerich et al., 2018] Schoelmerich, M. C., Katsyv, A., Sung, W., Mijic, V., Wiechmann, A., Kottenhahn, P., Baker, J., Minton, N. P., and Müller, V. (2018). Regulation of lactate metabolism in the acetogenic bacterium acetobacterium woodii. *Environmental Microbiology*, 20(12):4587–4595.

[Schuchmann et al., 2015] Schuchmann, K., Schmidt, S., Lopez, A. M., Kaberline, C., Kuhns, M., Lorenzen, W., Bode, H. B., Joos, F., and Müller, V. (2015). Nonacetogenic growth of the acetogen acetobacterium woodii on 1,2-propanediol. *Journal of Bacteriology*, 197(2):382–391.

[Semenova et al., 2011] Semenova, E., Jore, M. M., Datsenko, K. A., Semenova, A., Westra, E. R., Wanner, B., van der Oost, J., Brouns, S. J. J., and Severinov, K. (2011). Interference by clustered regularly interspaced short palindromic repeat (crispr) rna is governed by a seed sequence. *Proceedings of the National Academy of Sciences*, 108(25):10098–10103.

[Song et al., 2019] Song, C. W., Park, J. M., Chung, S. C., Lee, S. Y., and Song, H. (2019). Microbial production of 2,3-butanediol for industrial applications. *Journal of Industrial Microbiology and Biotechnology*, 46(11):1583–1601.

[Torres-Vinces et al., 2020] Torres-Vinces, L., Contreras-Zarazua, G., Huerta-Rosas, B., Sánchez-Ramírez, E., and Segovia-Hernández, J. G. (2020). Methyl ethyl ketone production through an intensified process. *Chemical Engineering & Technology*, 43(7):1433–1441.

[Weber et al., 2011] Weber, E., Engler, C., Gruetzner, R., Werner, S., and Marillonnet, S. (2011). A modular cloning system for standardized assembly of multigene constructs. *PLOS ONE*, 6(2):1–11.

[Wiedenheft et al., 2011] Wiedenheft, B., van Duijn, E., Bultema, J. B., Waghmare, S. P., Zhou, K., Barendregt, A., Westphal, W., Heck, A. J. R., Boekema, E. J., Dickman, M. J., and Doudna, J. A. (2011). Rna-guided complex from a bacterial immune system enhances target recognition through seed sequence interactions. *Proceedings of the National Academy of Sciences*, 108(25):10092–10097.

[Wood, 1991] Wood, H. G. (1991). Life with co or co2 and h2 as a source of carbon and energy. *The FASEB journal*, 5(2):156–163.

[Zhang et al., 2013] Zhang, Y., Heidrich, N., Ampattu, B. J., Gunderson, C. W., Seifert, H. S., Schoen, C., Vogel, J., and Sontheimer, E. J. (2013). Processing-independent crispr rnas limit natural transformation in neisseria meningitidis. *Molecular Cell*, 50(4):488–503.

Appendix A: HPLC Standards

Table 1: Preparation of HPLC standards.

Compound	Molar Mass [g/mol]	Target [mM]	Mass [g]	Vol. [mL]	Actual [mM]
Sodium formate	68.01	100	0.1395	20	102.6
Sodium formate	68.01	75	0.1038	20	76.3
Sodium formate	68.01	50	0.0660	20	48.5
Sodium formate	68.01	25	0.0448	25	26.3
Sodium formate	68.01	200	0.3502	25	205.7
Sodium formate	68.01	150	0.2685	25	157.6
Sodium formate	68.01	100	0.1870	25	109.9
Sodium formate	68.01	75	0.1050	20	77.2
Potassium formate	84.12	200	0.4312	25	205.3
Potassium formate	84.12	150	0.3399	25	161.8
Potassium formate	84.12	100	0.2142	25	102.0
Potassium formate	84.12	75	0.1300	20	77.2
Methanol	32.04	100	0.0641	20	100.0
Methanol	32.04	50	0.0321	20	50.0
Isopropanol (70%)	60.10	50	0.0675	25	44.8
Sodium acetate	82.03	100	0.1641	20	100.0
Propanal	59.10	1500	0.7566	10	1302
Propanal	59.10	1000	1.1600	20	998.0
Propanal	59.10	1000	1.1560	20	995.0
Propanal	59.10	50	0.0581	20	50.0

Appendix B: Primer

Table 2: Primers used in this study.

Primer Name	Sequence
KWO_113	TTGTCGACCTGTGATCATGCAAAATTAG
KWO_124	AAATTGATGACGATTAAGTATCATAATTGCAACGCCAAA
KWO_125	AAATTTTGGCGTTGCAATTATGATACTTAATCGTCATCA
KWO_126	AAATTGCGATTTTTTCAAGTGAAACCGGCAATTTATTAT
KWO_127	AAATATAATAAATTGCCGGTTTCACTTGAAAAAATCGCA
KWO_128	AAATTGATGACGATTAAGTATCATAATTGCAACGCCAAA
KWO_129	AAATTTTGGCGTTGCAATTATGATACTTAATCGTCATCA
KWO_130	GTATCGGGTCTCCAATTTGCTTATTTGATTTACATTATATAATATTG
KWO_131	CTCGATGGTCTCCCATGTTCATTTCCTCCCTTTAAATTTAAC
KWO_132	GTATCGGGTCTCCAATTCTAGTTTAGATTAATTCTTG
KWO_133	CTCGATGGTCTCCCATGTTGTTTCCTCCTAGTTG
KWO_134	GTATCGGGTCTCCCATGCGATTTTTTCAAGTGAAAC
KWO_135	CTCGATGGTCTCCAGCTCTCAATATCTGGCTGATCAC
KWO_136	GAATTCACCCTGTGAAGCAG
KWO_137	AATTCCCTTCTTATTGTCCG
KWO_139	TGAGTAAAGTATTGACTAGC
KWO_140	TGACCATTCCCTGGTCAGTG
REY_007	CTTGAGCGTCGATTTTTGTG
REY_008	GACTTTAAGCCTACGAATACC

Appendix C: Tools Used

- **ChatGPT (OpenAI, web access, free version)**
  Used for:
  - Assistance by translating from German to English
  - Improvement of English phrasing
  - Assistance with LaTeX code (e.g., `longtable`, `subfigure`)
  - Help with formulating appropriate search terms for literature searches on Google Scholar
  - Conversion of literature entries (e.g., `.ris` to `.bib`)
- **Google Translate**
  Used for:
  - Back translation from English to German
  - Translation of English sources to German for better understanding
- **Google Scholar**
  Used for literature searches and retrieving publications.
- **Overleaf**
  Preparation and management of the LaTeX manuscript
- **Zotero (version 7.0.30)**
  Management of bibliographic data
- **Thesis Template – TU Wien Informatics**
  LaTeX Template created by Thomas Auzinger (TU Wien Informatics), available at: `https://gitlab.com/ThomasAUZINGER/vutinfth`
- **Inkscape (version 1.4.2)**
  Used for labeling and preparing gel images for figures.
- **Chromeleon (version 7.3.2,Thermo Fisher Scientific)**
  Used for chromatographic data acquisition and analysis.
- **NanoDrop Software (version 3.8.1, Thermo Fisher Scientific)**
  Used for determining DNA concentration and purity via UV absorption.
- **NEB Tm Calculator**
  Used to estimate appropriate annealing temperatures PCR products (`https://tmcalculator.neb.com`).
- **Python (version 3.12.3)**
  Used for data analysis and visualization with the libraries `openpyxl`, `pandas`, `NumPy`, `SciPy`, and `Matplotlib`.
- **CLC Genomics Workbench (version 23, QIAGEN)**
  Used for sequence analysis.